Studying the Performance Enhancement Opportunities of Cooling Towers

Koh Chong Kai, John

A0184089R

Department of Mechanical Engineering

National University of Singapore

In partial fulfilment of the
requirements for the Degree of
Bachelor of Engineering
National University of Singapore

Acknowledgments

I would like to thank the National University of Singapore for giving me the opportunity to conduct a study on the optimization of cooling towers for my final year project.

I would like to express my deepest appreciation to my final year project supervisor, Dr. Md Raisul Islam for his continual support for the entire final year project. Dr. Raisul has provided me with an opportunity to research and study the effects of cooling towers and methods to optimize the towers. I greatly appreciate Dr. Raisul for arranging a time to meet me weekly for consultations and providing me with valuable insights on this project. I have greatly benefited from Dr. Raisul's guidance.

Table of Contents

1. Introduction

Today with our current technologies, Industrial plants, power plants, and buildings produce a lot of heat in operation. Hence, large air conditioning systems are put in place to reduce the amount of heat generated [1]. Mechanical equipment such as cooling towers is employed to expand waste thermal energy into the atmosphere via ambient air. Cooling towers are essentially a heat and mass transfer device that transfers thermal energy using direct contact between hot water and ambient air through fill packs [2]. For a mechanical cooling tower, a fan is used to provide a draft to move the air [3]. As cooling towers are an essential device to cool buildings, it is important to ensure that the cooling towers are optimized to suit different operating conditions. Thus, numerous studies and experiments have been conducted to improve heat and mass transfer through various methods and measures such as optimization of fill packs designs, methods to reduce ambient temperature or relative humidity of ambient air to changing thermophysical properties of operating fluid (water). Despite the vast applications of cooling tower designs proposed and developed all over the world, there are limited investigations and studies conducted in tropical climates such as Singapore. With the lack of studies conducted, analysis, and data, the lack of knowledge results in the high energy consumption of cooling towers in Singapore. This thesis will investigate on cooling tower operating conditions in Singapore, investigate potential methods of optimization of cooling tower, and propose a control strategy.

2. Literature review

2.1 Adding multi-walled carbon nanotubes to operating fluid of cooling tower

Extensive studies have been conducted to improve cooling tower performance while reducing energy consumption and water loss from evaporation and drift. Javadpour et al. showed how a current cooling tower's current cooling performance can be increased by adding multi-walled carbon nanotubes (MWCNTs) to the base operating fluid (water). Results have shown that the usage of nanofluids produced a higher cooling range and effectiveness as compared to using only water as their operating fluid [4]. However, one of the limitations to using MWCNTs is that an increase in the concentration of nanoparticles in cooling may lead to an increase in the likelihood of agglomeration of nanoparticles which results in a decrease of nanofluid heat transfer properties [4]. Hence, at higher nanoparticle flow rates, increasing nanoparticle

concentration does not have a significant effect on the cooling tower. The tower would be more effective if the use of nanoparticles at lower flow rates are used.

2.2 Utilizing water mist to cool ambient air at the inlet

Yang et al. investigated utilizing water mist as an evaporative as a pre-cooling measure to decrease the ambient air temperature. The study has shown that this method is environmentally friendly and energy-efficient that has the potential to improve and reduce efficiency and energy consumption [5]. On the other hand, a limitation to this method leads to the decrease in latent heat transfer between air and water. The effect of spraying mist to cool ambient air increases the relative humidity of the air. Hence, heat transfer will not be as effective as most of the heat transfer will be relying on sensible heat transfer between water and air.

2.3 Reducing makeup-water usage by harvesting fog fumes from cooling tower

Ghosh et al. studied a method to reduce make-up water usage by harvesting fog fumes that have been evaporated from the cooling tower. Results have shown that a superhydrophobic mesh at 15° inclination provides the best results for reducing make-up water usage. Advantages of a fog mesh include no change in external tower design, being environmentally friendly, and low maintenance cost. However, disadvantages of using a fog mesh could result in fog droplets deposited on mesh combines to form larger droplets and clog passages available for water to drain. As a result, impeding fog flows through the mesh which in turn prevents the further deposition of fog-laden droplets. In addition, droplet deposits can be lost through carry-over droplets that are swept downstream due to wind shear or prematurely dripping from mesh before reaching the water reservoir [6]. Hence, the above disadvantages attribute to an overall reduction of effectiveness in harvesting fog fumes from the cooling tower.

2.4 Optimizing spray nozzle design on cooling tower

Alkhedhair et al. investigated the optimization of spray nozzle design on cooling towers. Results have shown an improvement in cooling efficiency due to better spray dispersion. There was a 15% improvement in performance when the velocity of droplets was increased from 20 to 80m/s [7].

2.5 Switching cooling tower fill pack to elliptical finned tubes to improve cooling performance

Zhao et al. studied substituting cooling tower fill packing with the elliptical finned tube to improve thermal performance [8]. The process of heat and mass transfer is studied by numerical methods. Results have shown that the design of an elliptical finned tube can significantly improve thermal performance. A disadvantage to substituting a fill pack with finned tubes

would be an increase in space usage and the possible increase in power consumption due to extra motors used to circulate water through the finned tubes.

2.6 Flexible fill pack design that changes configurations according to weather conditions

Yu proposed a plate-heat-exchanger packing design to operate flexibly under different ambient conditions to improve water savings. Results have shown that cooling towers have high water savings annually, up to 21.5% water savings [9]. Advantages of having a flexible packing design would be, the cooling tower will be able to adapt to different ambient conditions (summer, winter, etc.), reducing the evaporation loss significantly. However, this design will not be as applicable and effective for tropical countries such as Singapore as it experiences a constant ambient condition all year round.

2.7 Fill pack design with fill pack configurations for cooling tower

Dmitriev et al. experimented on the effects of different types of fill packs in cooling towers for inclined-corrugated contact elements of 5mm hole and 6mm hole. Results show that fill the pack with a 6mm hole was most efficient as it provides a higher value of heat and mass transfer coefficient [10].

2.8 Experimentation of filters to minimize evaporation loss from cooling tower

Shublaq et al. experimented on different types of filters to help reduce evaporation loss from cooling towers. Results are shown for evaporation loss reduction: aluminum filter – 17%, pre-filter – 14.3%, glass fiber – 13%, and pocket filter – 11.3%. The advantages of using such filters have little change in tower design while increasing the efficiency of tower water savings [11]. The disadvantage of using filters would be the filters capture water droplets that are entrained in the airstream by condensation. However, these filters do not capture moisture in vapor form. Hence, then it will not be separated by any filter. For moisture separation to occur, the temperature of air must be cooled down below dew point temperature for condensation to occur. Thus, this may not be as effective as the filters cannot prevent evaporation loss from vapor form.

2.9 Cooling tower with the liquid desiccant system to reduce the relative humidity of ambient air

Gilani et al. developed a shower cooling tower with a counter-current flow pattern and a liquid desiccant system equipped with an internal cooling system. Results have shown that the hybrid system can reduce water temperature from 44°C to about 32°C [12].

2.10 Rotational cooling tower

Amini et al. experimented on the performance of rotational splash-type packing cooling towers. Results have shown that when rotational packing rotates with higher rotating velocity, more heat is rejected. When the rotation velocity of the fill pack is increased from 0 – 17 RPM, heat rejection increased about 23% [13]. A disadvantage to having a rotational fill pack is the high motor power consumption required to move a fill pack.

2.11 Harvesting rainwater as a form of make-up water for cooling tower

Thomé analyzed utilizing rainwater as a form of makeup water to reduce water consumption [14]. The disadvantage of utilizing this method is, rainfall might be inconsistent in certain regions of Singapore, as the storage tank may not be fully utilized all year round. In addition, external ground space is required to collect rainwater, which most places in Singapore do not have.

2.12 Modification of cooling tower with high precision airflow regulation method

Dehaghani studied a Parallel Path Wet/Dry with a high-precision airflow regulation method that can be modified onto an existing cooling tower. Results showed that with the high-precision airflow method, fan power consumption was decreased by 64% and water consumption rate decreased by 9.4% [15].

2.13 Dew point evaporative cooling tower

Fan et al. experimented on a dew point evaporative cooling tower (DPECT) based on M-cycle. Results have shown that DPECT can reduce water outlet temperature below the wet-bulb ambient temperature of air [16]. However, a disadvantage to DPECT is that the fan consumption of the cooling tower would be high. In the DPECT, there were a few 90° turns to move air around the cooling tower. This causes pressure will drop, resulting in high power consumption to maintain constant pressure in the cooling tower.

2.14 Cooling tower fill pack with ribs packing

Shahali et al. experimented on various numbers of ribs packing in the cooling tower to improve cooling tower performance. Results have shown that among the investigated parameters of inlet water temperature, number of PVC ribs packing and mass flow rate of air, the mass flow rate of air is the most effective parameter to enhance efficiency [1].

2.15 Alternative materials as fill for cooling tower

Tomás et al. experimented on alternative materials such as coconut husks, coconut fiber and Polyethylene Terephthalate (PET) for cooling tower fills. Results have shown that alternative fill materials are not able to cool water as effectively as industrial fill materials. However, with

the low cost and environmentally friendly materials, alternative fill materials suggest that these materials have the potential to be used fills for cooling towers [17].

2.16 Wire mesh fill packing for cooling tower

Kumar et al. investigate the use of the new type of wire mesh packings for improving the performance of the conventional liquid desiccant spray tower. Results have shown that wire mesh packings have improved conventional spray towers by 30%. Advantages are low cost, improves efficiency, and have a zero carry-over of liquid desiccant [18]. On the other hand, the mesh packings are designed only for liquid desiccant cooling towers. Hence, it will not be as effective when the mesh technology is applied on cooling towers that do not have employ liquid desiccant in their cooling tower.

3. Primary objectives

1. Develop a simple theoretical model on heat and mass transfer mechanisms involving in a counter–flow cooling tower.
2. Conduct parametric studies to analyze the effects of different operating and design parameters that controlled the performance of cooling towers.
3. Develop a simulation on ANSYS fluent
4. Develop an ambient air precooler configuration on ANSYS fluent
5. Develop a neural network to predict cooling tower outlet conditions
6. Propose a control strategy to optimise overall energy consumption of the cooling towers

4. Mathematical modelling

Figure 0 shows a schematic of how water is cooled from inlet when it is flowing along two plates.

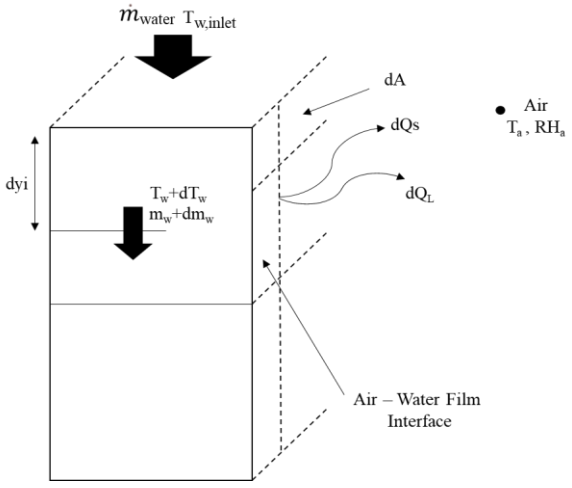

Figure 0. Schematic of water being cooled from top of plate

A numerical model was developed based on the energy-mass balance between water and air. The following assumptions are used to simplify the model.

1. Adiabatic evaporative cooling process [air humidification and cooling of water]
2. Changes in mass flow rates of ambient air and water are negligible
3. The system is in a steady-state condition
4. The system is in a steady-state condition
5. Heat and mass transfer between air and water interface area is equal to the area of packing

Sensible heat transfer rate from control element:

$$dQ_S = hc\,dA(Tw - Ta) \quad [1]$$

Latent heat transfer rate from control element:

$$dQ_L = \dot{m}_v h_{fg} dA$$
$$dQ_L = hm(m_{fis} - mfia)h_{fg}dA \quad [2]$$

Energy balance for water:

Energy lost by water = latent heat gained by air + sensible heat gained by air + energy lost by water from change in mass

$$\mathrm{C_p T_w}\frac{dm_w}{\mathrm{dA}} + \mathrm{mwCp}\frac{\mathrm{dT_w}}{\mathrm{dA}} = -\mathrm{hc(T_w - Ta)} - \{\mathrm{hm(m_{fis} - mfia)h_{fg}}\} \quad [3]$$

Water evaporation rate:

$$\frac{d\dot{m}_v}{dA} = hm(mfis - mfia) \quad [4]$$

Change in mass flow rate of water:

$$\frac{d\dot{m}_w}{dA} = -hm(mfis - mfia) \quad [5]$$

Combining change in mass flow rate of water [5] and energy balance for water [3] equation:

$$\frac{dT_w}{dA} = \frac{1}{m_w C_p}\{-hc(T_w - Ta) + hm(m_{fis} - mfia)(C_p T_w - hfg)\} \quad [6]$$

Where mass fraction of water vapor at saturated section of water film:

$$\mathrm{m_{fis}} = \frac{\rho_{vis}}{\rho_s} \quad [7]$$

Density of water vapor at saturated section of water film:

$$\rho_{vis} = \frac{(Psat_{at\ TW})Mv}{R_u T_w} \quad [8]$$

Total density of saturated water vapor:

$$\rho_s = \frac{(P_{sat\ at\ TW})\,M_V}{R_u T_w} + \frac{(P_{atm} - P_{sat\ at\ TW})\,M_a}{R_u T_w} \quad [9]$$

Mass fraction of water vapor in air:

$$\mathrm{m_{fiair}} = \frac{\rho_{viair}}{\rho_{air}} \quad [10]$$

Density of water vapor in air:

$$\rho_{viair} = \frac{(RH)(Psat_{at\ Ta})Mv}{R_u T_w} \quad [11]$$

Density of air:

$$\rho_{air} = \frac{(RH)(P_{sat\ at\ Ta})\,M_V}{R_u T_a} + \frac{(Pat_m - RH\ x\ P_{sat\ at\ Ta})\,M_a}{R_u T_w} \quad [12]$$

Sensible energy balance of air:

$$m_a Cp_a T_{\mathrm{ao}} = \mathrm{m_a Cp_a T_{ai}} + \mathrm{h_c dA(T_w - T_a)} \quad [13]$$

Moisture balance of air:

$$m_a \omega_{ao} = m_a \omega_{ai} + dAh_m(mfis - mfia) \quad [14]$$

Absolute humidity:

$$RH = \frac{\omega \mathrm{Patm}}{Psat(0.6219 + \omega)} \quad [15]$$

5. Initial condition

Table 1 shows the base operating parameters used for numerical simulations on MATLAB program.

Table 1. Operating parameters for MATLAB numerical simulation

Parameter	Value	Unit
Air Velocity, Inlet	2.75	m/s
Air Temperature, Inlet	29	°C
Relative Humidity of ambient air	0.84	%
Molecular Weight of Air	29.0	kg/mol
The temperature of Water	35.0	°C
Water Flow Rate	0.0136	kg/s
Molecular Weight of Water	18	kg/mol
Specific Heat Capacity of Water	4200	J/kg.K
Number of elements	100	N.A
height of control element	0.03	m
width of control elements	0.1	m

6. Runge – Kutta (RK) method

As equations [5] and [6] is a 1st order ordinary differential equation, they can be solved simultaneously using the 4th order Runge – Kutta (RK4) method. The function of the RK4 method can be defined as:

$$y' = \frac{dy}{dA} = f(A, y)$$

Where function $f(A, y)$ is the inlet conditions. $\frac{dy}{dA}$ is used to demonstrate the change in air temperature, water temperature, and mass flow rate over the change in the area. The equations show RK4 equations used to solve $\frac{dy}{dA}$.

4th order Runge – Kutta (RK4) method:

$$k_1 = \Delta \mathrm{A}.\, f(\mathrm{A} = \mathrm{A}_0, \mathrm{y} = \mathrm{y}_0) \qquad [1]$$

$$k_2 = \Delta A.\, f(A = A_0 + \frac{\Delta A}{2}, y = \frac{y_0 + k_1}{2}) \quad [2]$$

$$k_3 = \Delta A.\, f(A = A_0 + \frac{\Delta A}{2}, y = \frac{y_0 + k_1}{2}) \quad [3]$$

$$k_4 = \Delta A.\, f(A = A_0 + \Delta A,\ y = y_0 + k_3 \quad [4]$$

$$y_1 = y_0 + \frac{k_1 + k_2 + k_3 + k_4}{6} \quad [5]$$

Increment of RK4 method

$$A_0 = A_0 + \Delta A \quad [6]$$

$$y_0 = y_1 \quad [7]$$

The equations are then performed repeatedly from the initial conditions to the end of plate length or width. At the end of the plate length or width, outlet conditions are found. The increment can be calculated simply by the length or width of the plate divided by the number of iterations desired.

7. Design parameter

Table 2 below shows the design parameters used in MATLAB numerical simulation.

Table 2. Design Parameters on MATLAB

Design Parameter	Value	Unit
Width of Plate	1.0	m
Length of Plate	3.0	m
Area of control Element	Length Control Number * Width	m^2
Area of control Element	Length Control Number * height	m^2

8. MATLAB model

A MATLAB program was developed to solve the above-mentioned equations and the RK4 method. With the input parameters, the program will keep the parameters constant while using

the RK4 method to solve for the outlet temperature of water and air. The Figure 1 shows the program logic of the MATLAB program. After the required parameters are input into the program (T_{ai}, T_{wi}, RH, m_w, T_{av}), the program will solve the RK4 method by using multiple for loops for the calculation of $T_{a,}$ T_w, RH, $m_{w,}$ and T_{av} at each grid point. At the end of 100 by 10 iterations, final T_a, T_w, RH, $m_{w,}$ and T_{av} are calculated.

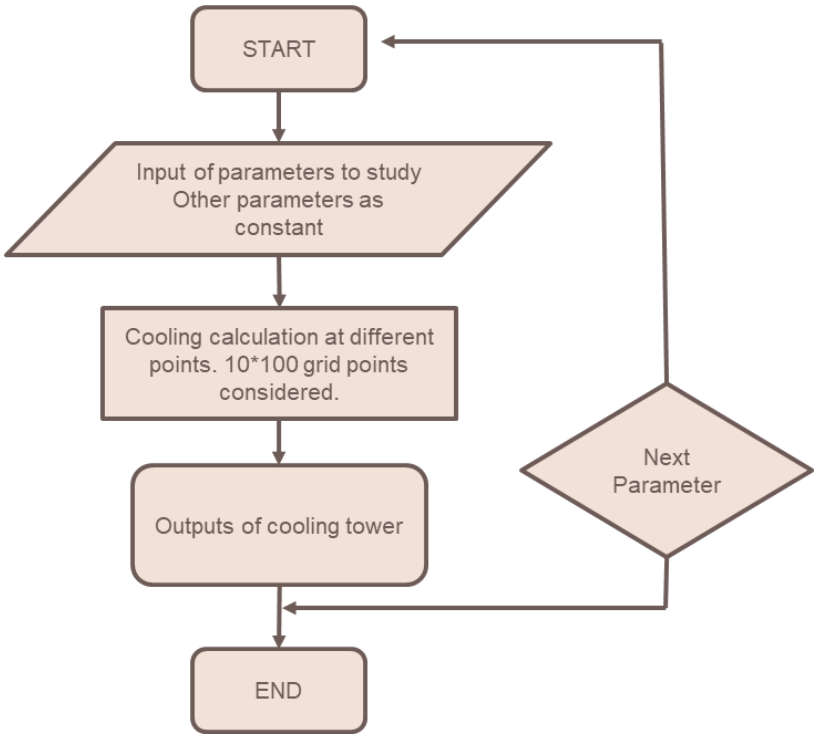

Figure 1. MATLAB flow chart program

9. ANSYS (fluent) model

9.1 Geometry

A three-dimensional model was designed on the DesignModeler of a crossflow fill. Figure 2 illustrates how the plates were designed 3m by 1m and containing a gap of 15mm in between the plates.

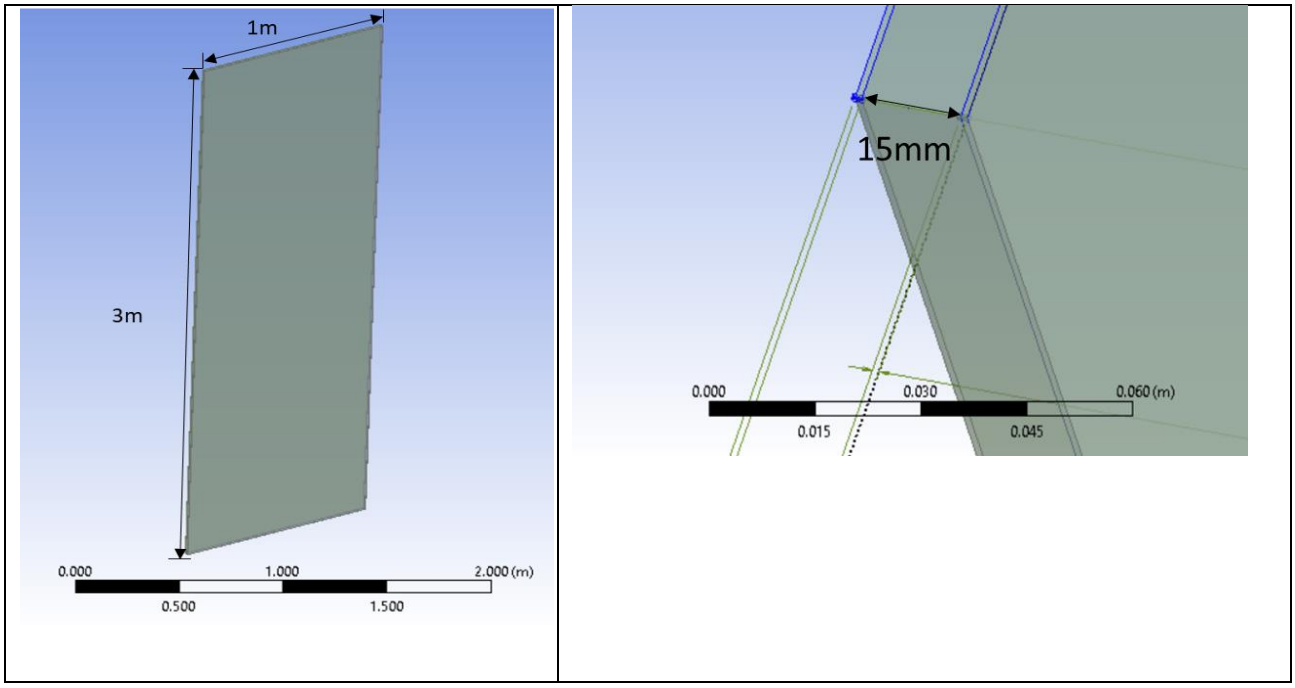

Figure 2. 3-Dimensional design of on DesignModeler

9.2 Mesh

Due to the student mesh limit size of 512,000 cells/nodes, the element size of the mesh was set to 0.05m. Water was introduced at the top of the plate while air is introduced at the side of the plate. Figure 3 illustrates the mesh of 3-D model and boundary conditions.

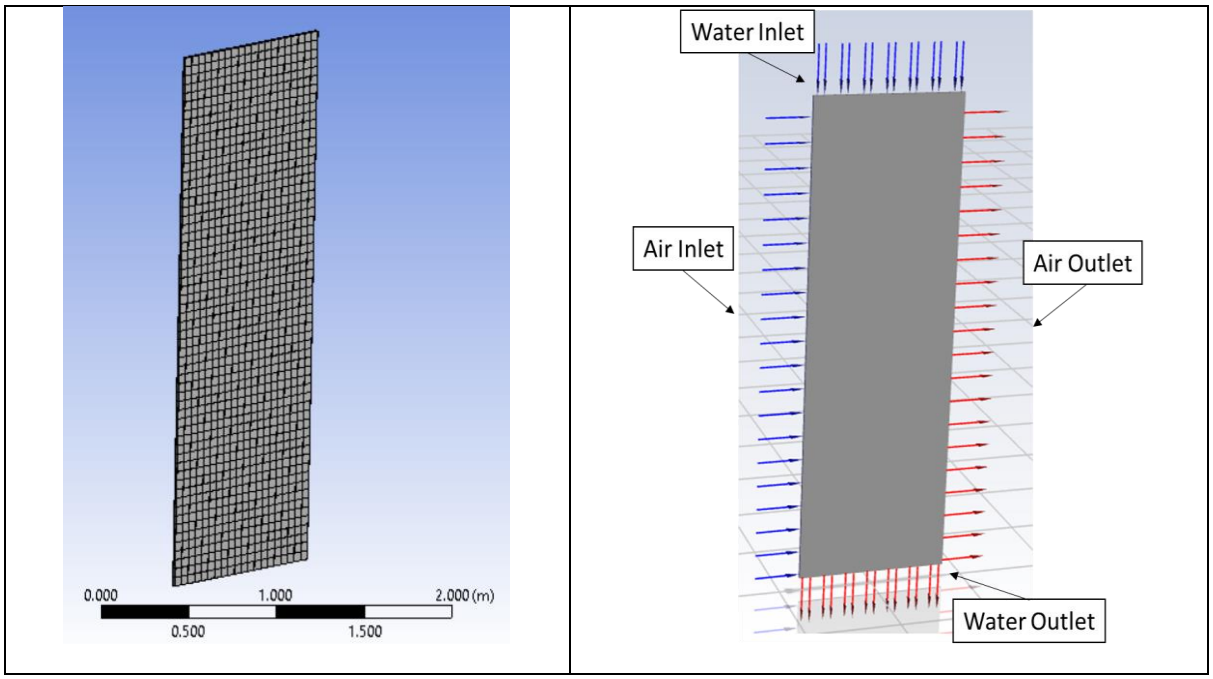

Figure 3. 3-D mesh model and boundary conditions

9.3 Set-up

As the flow velocity and mass flow rate are low and incompressible, a pressure-based solver is used as a solution algorithm. The flow is set to laminar flow. Mass transfer between saturated air at bulk water temperature and ambient air is simulated by solving species transport without reaction. For heat transfer analysis, the energy equation is enabled. For the continuous phase, steady flow transport equations are solved. For pressure-velocity coupling, a coupled algorithm is used for accuracy and numerical stability. Discretization of equations are solved using a second-order upwind scheme [19].

9.4 Inlet conditions

Table 3 shows the inlet operating conditions on ANSYS fluent.

Table 3. Inlet operating conditions

Parameter	Value	Unit
Air Velocity, Inlet	2.75	m/s
Air Temperature, Inlet	29	°C
Relative Humidity of ambient air	0.84	%
Mass Fraction of air	0.021	kg/kg
The temperature of Water	35.0	°C
Water Flow Rate	0.0136	kg/s

Figure 4 shows the temperature gradient of water and relative humidity after simulation.

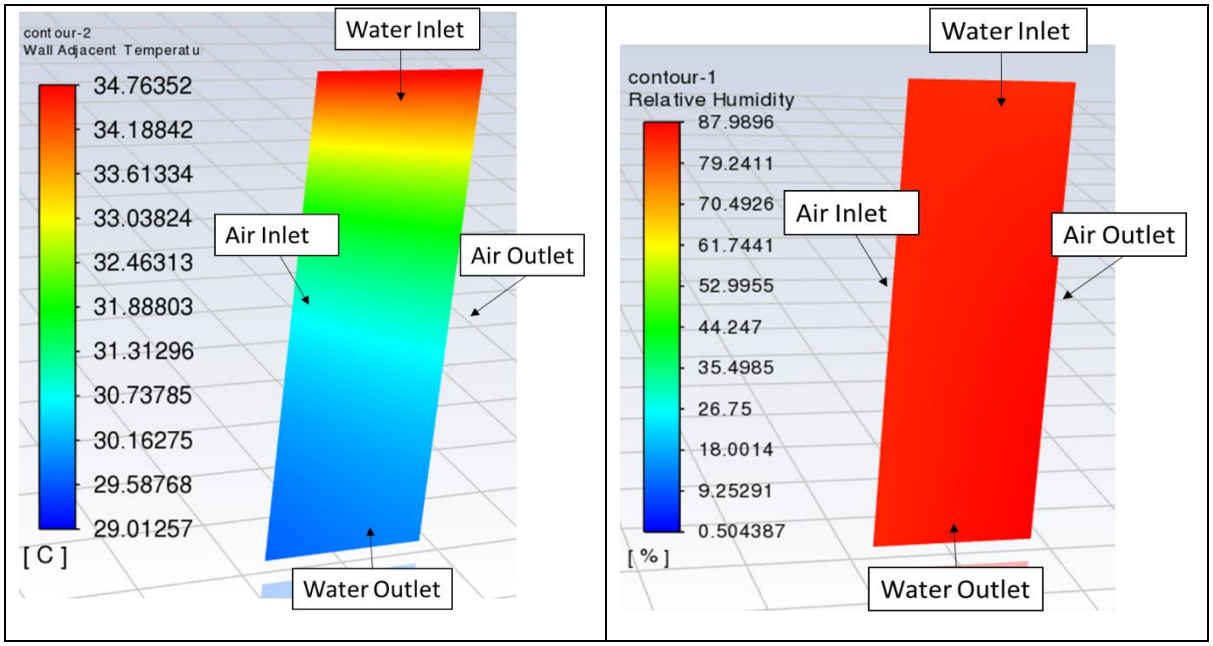

Figure 4. Temperature gradient of water and relative humidity

10. Validation of numerical model

With the developed theoretical MATLAB and ANSYS (fluent) model, both models are compared with data from [20] for validation of data. Table 4 shows the inlet operating conditions from published literature. In table 6, the average values of error for both models are less than 5%. Hence, both theoretical model on MATLAB and ANSYS (fluent) shows good agreement with published literature. Table 5 shows the outlet conditions from MATLAB, ANSYS fluent and published literature. Figure 5 shows the air outlet temperature and Figure 6 shows the water outlet temperature of MATLAB, ANSYS and published literature.

Table 4. Inlet operating conditions from published literature

No. of Data	T_{ai} (°C)	T_{wb} (°C)	RH (%)	T_{wi} (°C)	$\dot{m}_a$ (kg/m^{2}s)	$\dot{m}_a$ (kg/m^{2}s)
1	24.8	20.1	65.3	30.3	0.0144	0.0131
2	25.3	20.9	67.7	32.9	0.0144	0.0131
3	27	22	59.3	36.6	0.0144	0.0131
4	25.1	20.8	68.2	30.4	0.0144	0.0107
5	25.1	21.1	70.3	30.2	0.0144	0.0082

Table 5. Outlet temperatures of MATLAB, ANSYS and published literature

No. of Data	MATLAB		ANSYS		PUBLISHED LITERATURE	
	T_{ao} (°C)	T_{wo} (°C)	T_{ao} (°C)	T_{wo} (°C)	T_{ao} (°C)	T_{wo} (°C)
1	24.8	26.6	25.2	28.7	24.2	26.7
2	25.3	28.3	25.9	30.0	25.3	28.8
3	27.0	30.4	27.7	32.5	27.3	31.2
4	25.1	26.3	25.5	28.1	24.4	26.6
5	25.1	25.5	25.3	27.1	24.2	26.1

Table 6. percentage of error between MATLAB, ANSYS

No. of Data	MATLAB		ANSYS	
	T_{ao} (°C)	T_{wo} (°C)	T_{ao} (°C)	T_{wo} (°C)
1	2.51	0.47	4.21	4.21
2	0.05	1.65	2.25	2.25
3	1.04	2.47	1.58	1.58
4	2.89	1.29	4.51	4.51
5	3.74	2.38	4.42	4.42
Average Error (%)	2.05	1.65	3.39	3.39

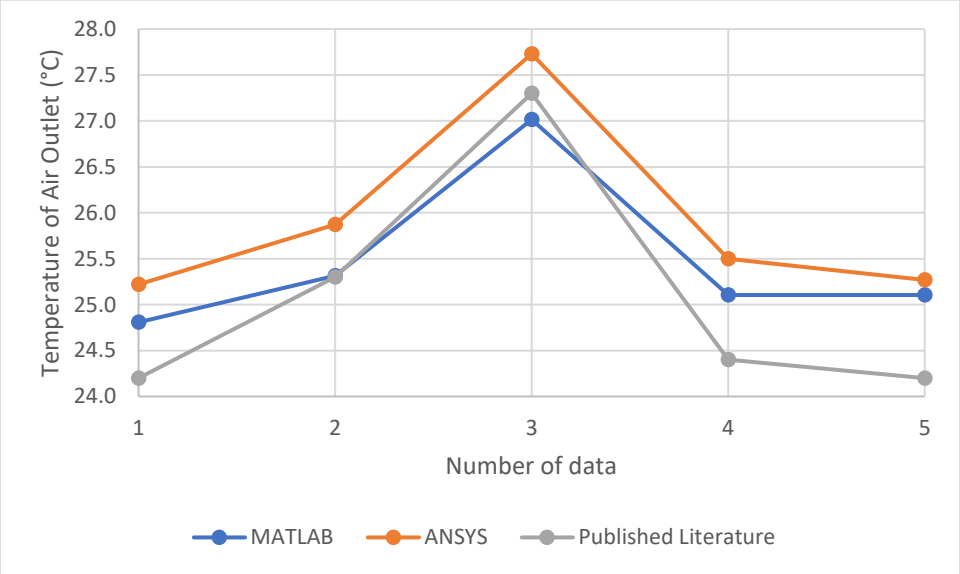

Figure 5. Air outlet temperature of MATLAB, ANSYS and published literature

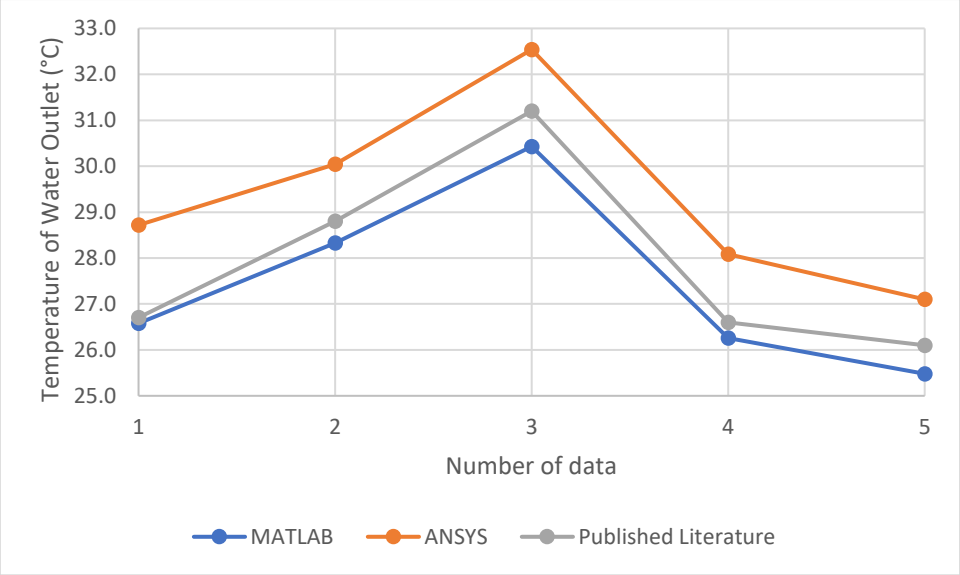

Figure 6. Water outlet temperature of MATLAB, ANSYS and published literature

11. MATLAB Parametric studies

A parametric study was conducted on MATLAB to examine how hot water is cooled to form 40◦C. Table 7 shows the reference inlet conditions before the parametric study was conducted.

Table 7. Reference inlet conditions

Reference Parameters	Value	Units
Relative Humidity:	84	%
Air Velocity inlet	2	m/s
Temperature Air inlet:	30	◦C
Temperature water inlet:	40	◦C
Water flow rate inlet:	0.011	kg/s

11.1 Effects of varying drying air velocity

By varying different drying air velocities from 0.5 - 5 m/s, it was observed that there was a decrease in water outlet temperature when air velocity was increased. When air velocity increases, the temperature difference at the outlet becomes less prominent. At 3 to 5m/s the change in water temperature was not as significant as compared to the initial change in temperature from varying air velocity from 0.5 to 1.5 m/s. Table 8 shows the change in parameter for drying air velocity. Figure 7 shows variations of water temperature along the length of plate for different values of drying air velocity.

Table 8. Change in inlet parameter for drying air velocity

Parameters	Value	Units
Drying Air Velocity	0.5 - 5	m/s
Relative Humidity:	84	%
Temperature Air inlet:	30	◦C
Temperature water inlet:	40	◦C
water flow rate inlet:	0.011	kg/s

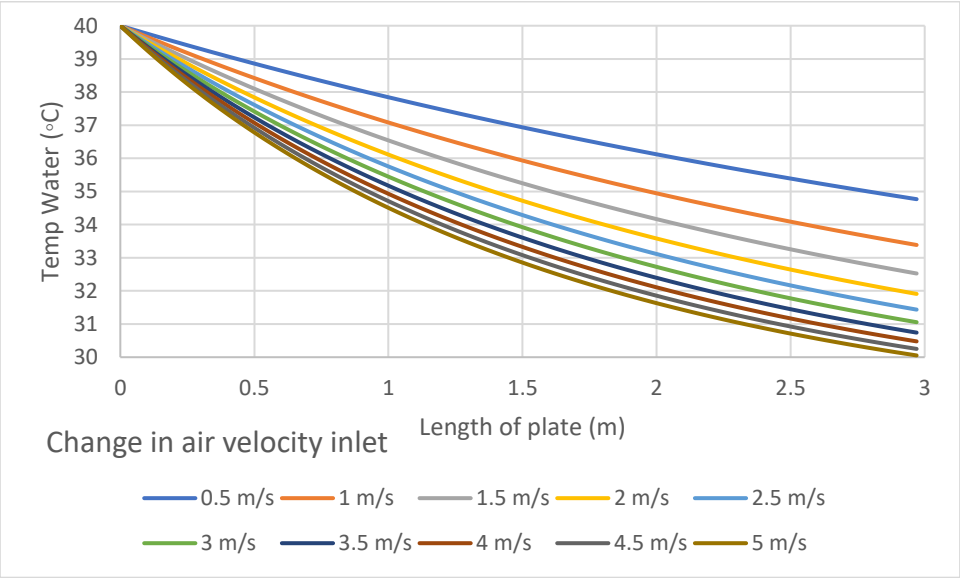

Figure 7. Water temperature along length of plate

11.2 Effects of varying relative humidity

As the relative humidity of air varies from 84 to 10%, it was observed that water temperature drops drastically. Table 9 shows the change in parameter for relative humidity. Figure 8 shows the variations of water temperature along the length of plate for different values of relative humidity.

Table 9. Change in inlet parameter for relative humidity

Parameters	Value	Units
Drying Air Velocity	2	m/s
Relative Humidity:	84 – 10	%
Temperature Air inlet:	30	◦C
Temperature water inlet:	40	◦C
water flow rate inlet:	0.011	kg/s

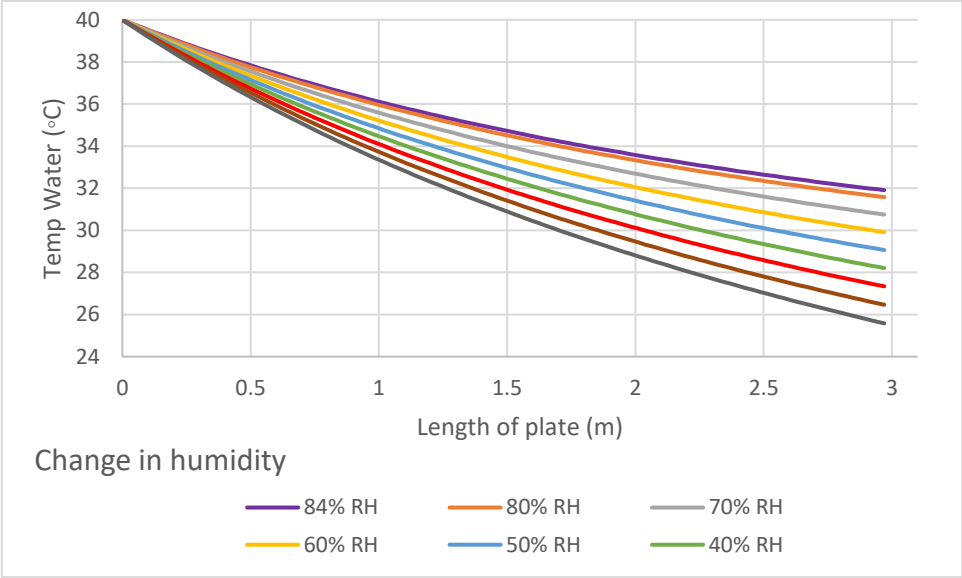

Figure 8. Water temperature along length of plate

11.3 Effects of varying temperature air at inlet

By varying air temperature at the inlet from 32 - 18 °C, it was observed that the temperature gradient decreases as the temperature of the air inlet decreases. Table 10 shows the change in parameter for air temperature inlet. Figure 9 shows the variations of water temperature along the length of plate for different values of temperature of air at inlet.

Table 10. Change in inlet parameter for temperature of air inlet

Parameters	Value	Units
Drying Air Velocity	2	m/s
Relative Humidity:	84%	%
Temperature Air inlet:	18 – 32	◦C
Temperature water inlet:	40	◦C
water flow rate inlet:	0.011	kg/s

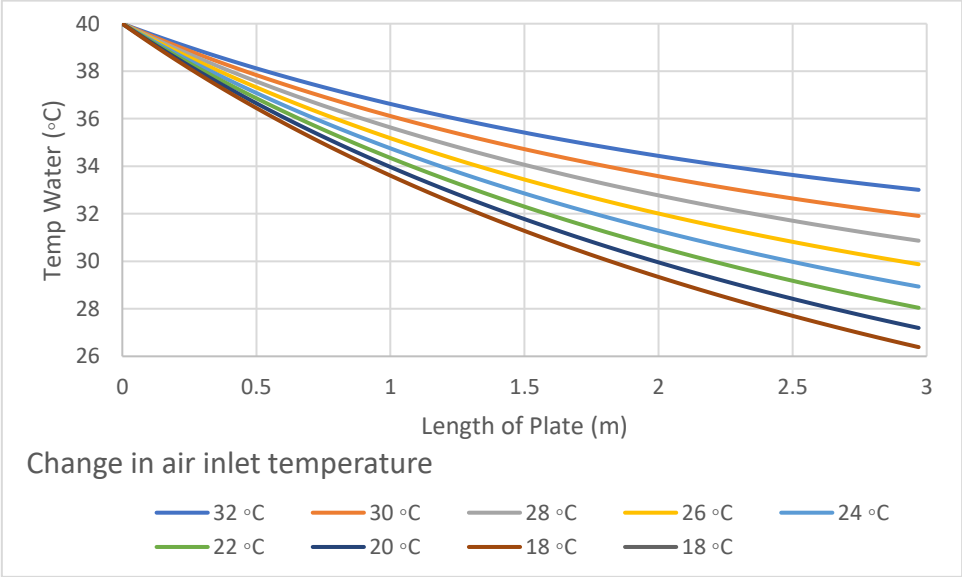

Figure 9. Water temperature along length of plate

11.4 Effects of varying water flow rate at inlet

By varying the water flow rate at the inlet, a significant drop in water temperature was observed when the mass flow rate of water was in the range of 0.011– 0.5 kg/s. Table 11 shows the change in parameter for water flow rate at inlet. Figure 10 shows the variations of water temperature along the length of plate for different values of temperature of air at inlet.

Table 11. Change in inlet parameter for water flow rate

Parameters	Value	Units
Drying Air Velocity	2	m/s
Relative Humidity:	84	%
Temperature Air inlet:	30	◦C
Temperature water inlet:	32	◦C
water flow rate inlet:	0.011 – 0.5	kg/s

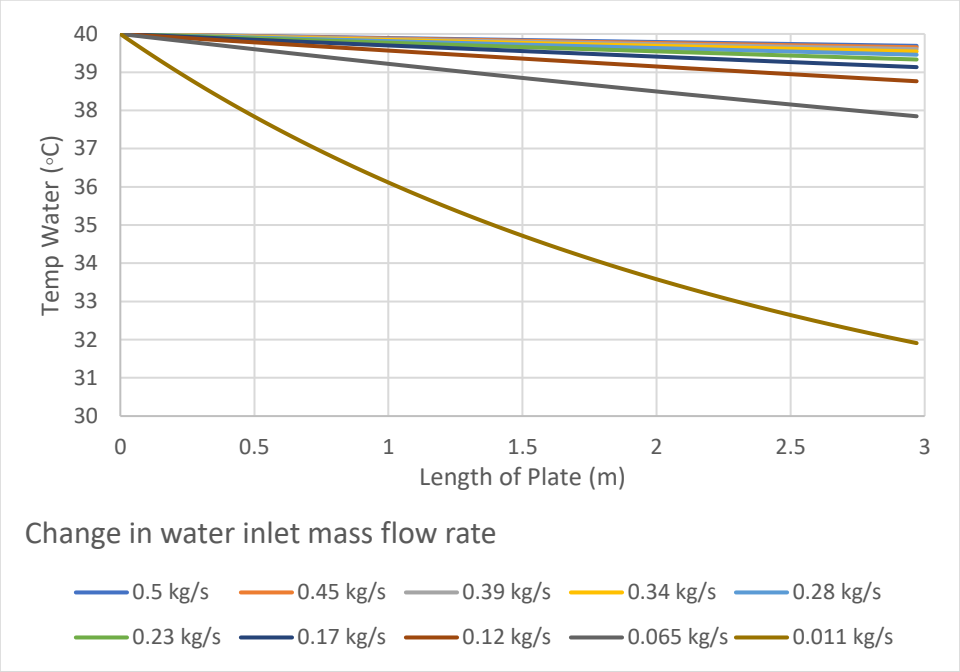

Figure 10. Variation of water temperature along length of plate with differing water flow rates

11.5 Effects of varying water inlet temperature

It was observed that when the temperature of water decreases, the temperature gradient of water decreases. Table 12 shows the change in parameter for water inlet temperature. Figure 11 shows the variations of water temperature along the length of plate for different values of temperature of water inlet temperature.

Table 12. Change in inlet parameter for water inlet temperature

Parameters	Values	Units
Drying Air Velocity	2	m/s
Relative Humidity:	84	%
Temperature Air inlet:	30	◦C
Temperature water inlet:	40 – 30	◦C
water flow rate inlet:	0.011	kg/s

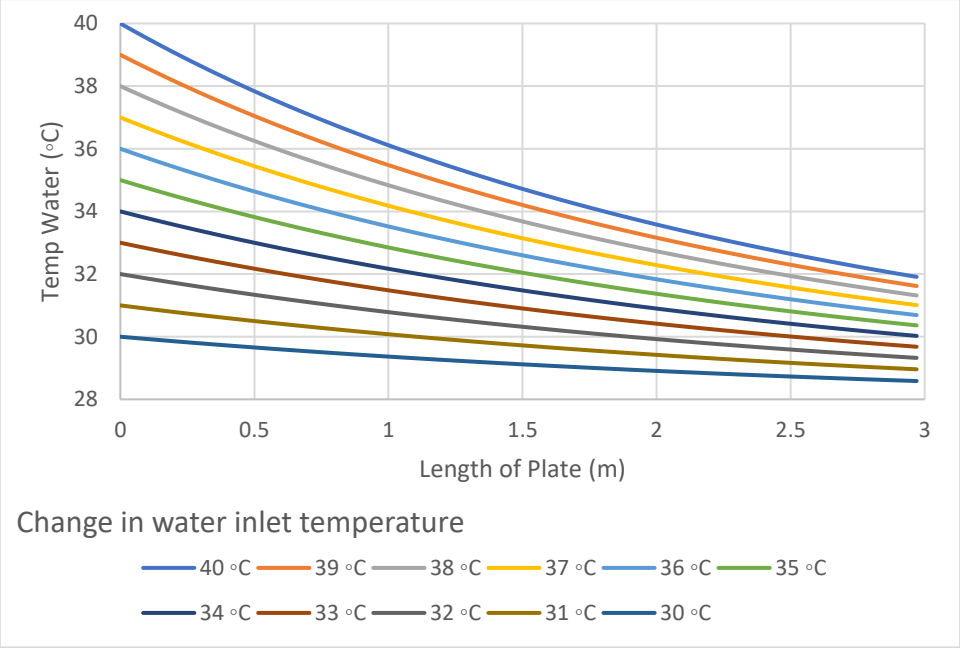

Figure 11. Water temperature along length of plate

12. ANSYS (Fluent) Parametric studies

Upon completing MATLAB simulations, ANSYS simulations were conducted to investigate how different height designs of cooling tower, water inlet velocity, air inlet velocity would affect air and water temperature. Table 13 shows the reference conditions of parameters before the parametric study was conducted.

Table 13. Reference inlet conditions

Reference Parameters	Values	Units
Height of plate	3	m
Width of plate	1	m
Gap between plates	15	mm
Water film thickness	1	mm
Relative Humidity:	84	%
Mass Fraction	0.022	kg/kg
Air Velocity inlet	2	m/s
Temperature air inlet:	30	◦C
Temperature water inlet:	40	◦C
Water flow rate inlet:	0.011	kg/s

12.1 Effects of varying cooling towers height

When varying the height of the cooling tower, it was observed that the cooling tower height at 1m has the least amount of cooling as compared to the other tower height. Table 14 shows the change in parameter for tower height. Figure 12, 13, 14, 15 and 16 shows the variations of water temperature along the length of plate for different values of tower height.

Table 14. Change in inlet parameter for tower height

Parameters	Values	Units
Height	1 – 3	m
Air Velocity inlet	2	m/s
Temperature Air inlet:	30	◦C
Temperature water inlet:	40	◦C
Water flow rate inlet:	0.011	kg/s

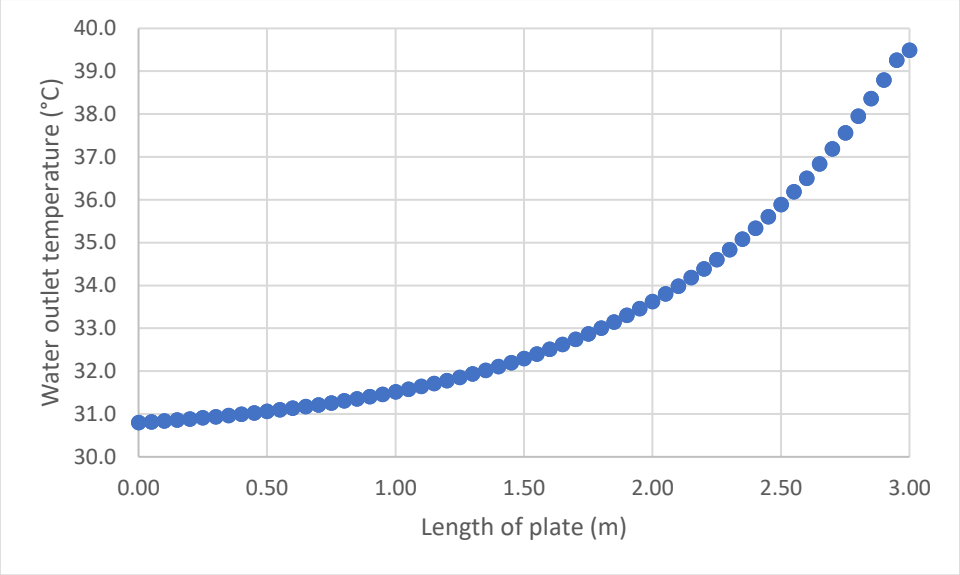

Figure 12. Variation of water temperature along 3m length of plate

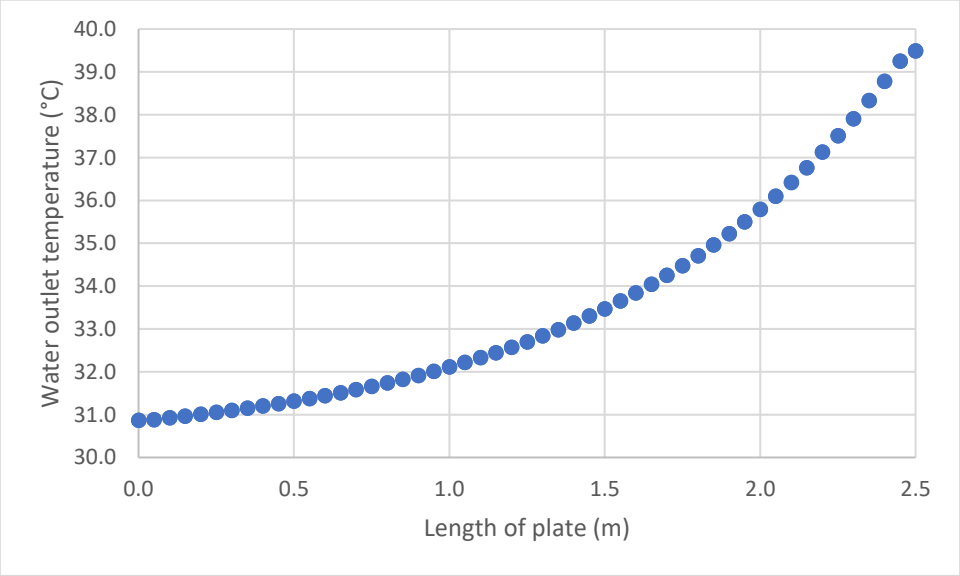

Figure 13. Variation of water temperature along 2.5m length of plate

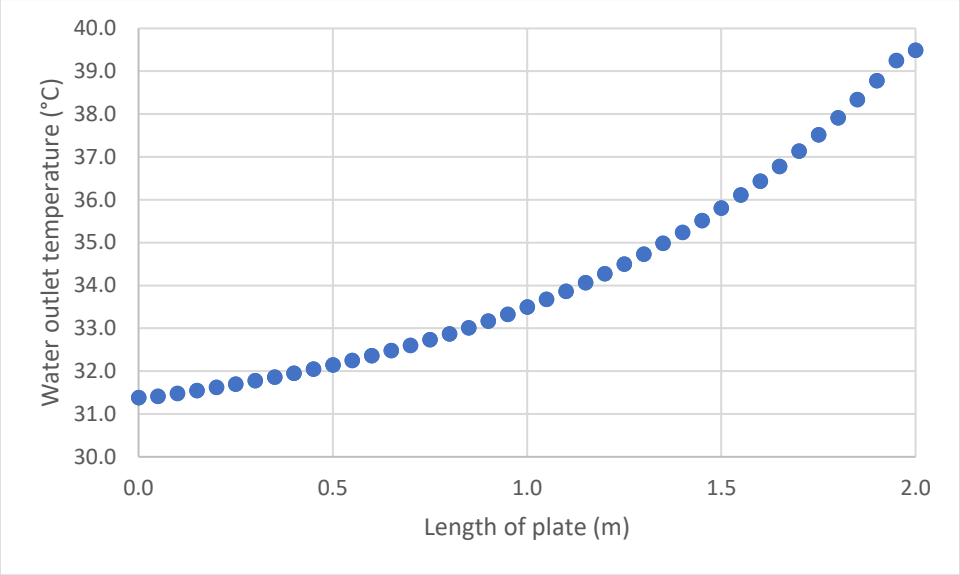

Figure 14. Variation of water temperature along 2m length of plate

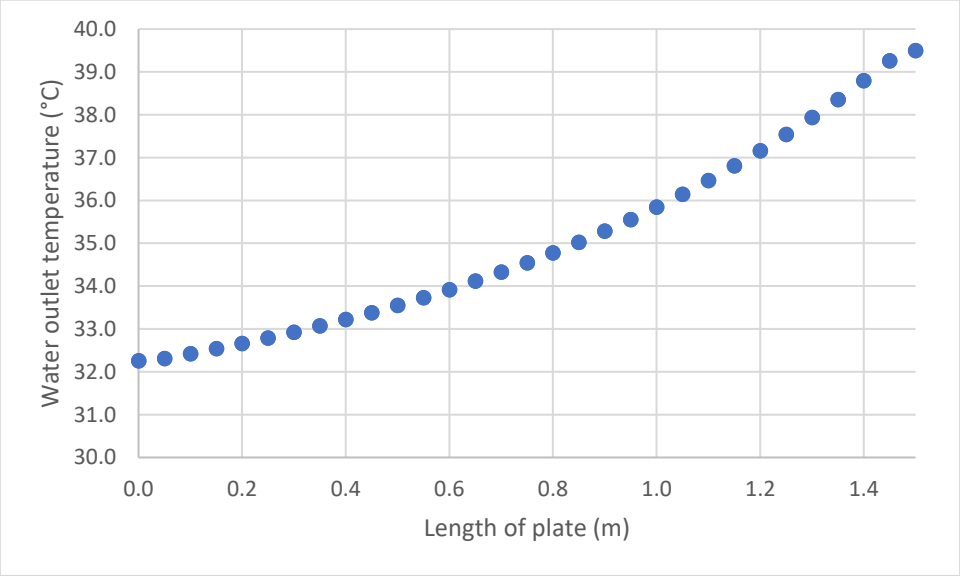

Figure 15. Variation of water temperature along 1.5m length of plate

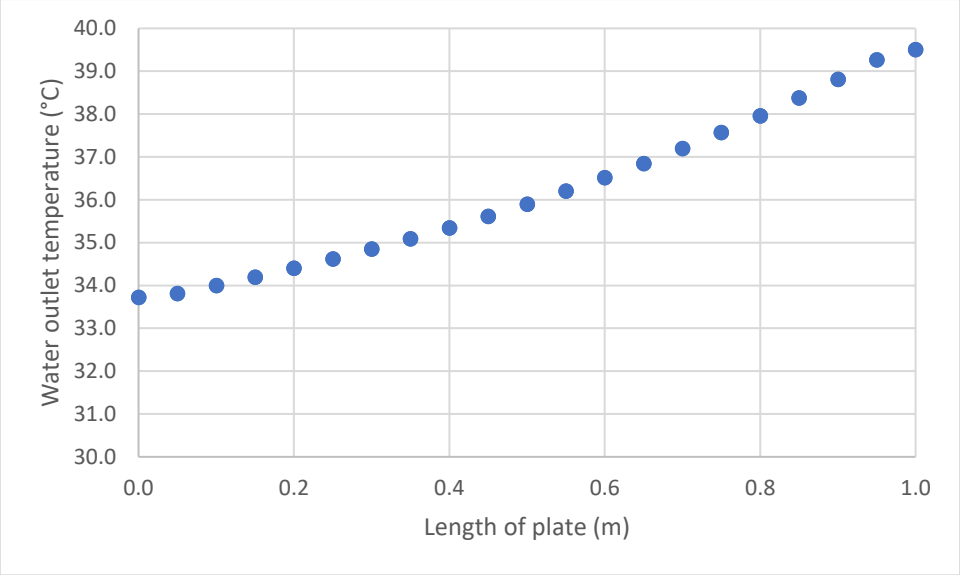

Figure 16. Variation of water temperature along 1m length of plate

12. 2 Effects of varying water mass flow rate

When varying water inlet mass flow rate, the mass flow rate that is the lowest have the highest amount of cooling. It is also observed that there is an increase in temperature gradient when the mass flow rate decreases. Table 15 shows the change in parameter for mass flow rate. Figure 17 shows the variations of water temperature along the length of plate for different values of water mass flow rates.

Table 15. Change in inlet parameter for water mass flow rate

Parameters	Values	Units
Height	3	m
Air Velocity inlet	2	m/s
Temperature Air inlet:	30	◦C
Temperature water inlet:	40	◦C
Water flow rate inlet:	0.006 – 0.0210	kg/s

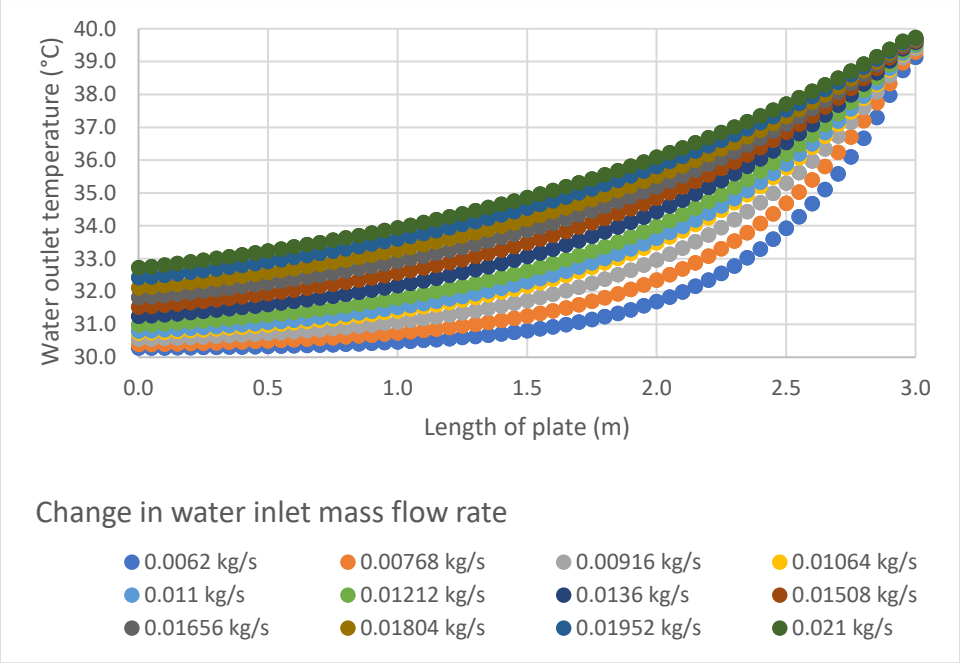

Figure 17. Variation of water temperature along length of plate with differing water mass flow rate

12.3 Effects of varying water inlet temperature

It is observed that water at different inlet temperatures has been cooled approximately to the same water outlet temperature. Table 16 shows the change in parameter for water inlet temperature. Figure 18 shows the variations of water temperature along the length of plate for different values of water inlet temperatures.

Table 16. Change in inlet parameter for water inlet temperature

Parameters	Values	Units
Height	3	m
Air Velocity inlet	2	m/s
Temperature Air inlet:	30	◦C
Temperature water inlet:	30 – 40	◦C
Water flow rate inlet:	0.011	kg/s

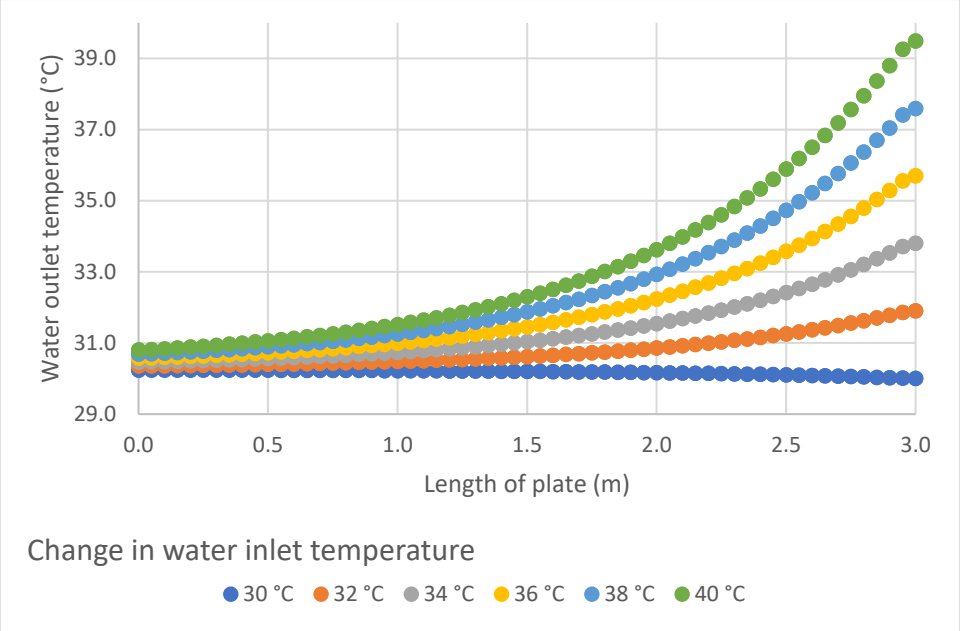

Figure 18. Variation of water temperature along length of plate with differing water inlet temperature

12.4 Effects of varying airflow velocity

When varying air inlet velocity from 0.5 – 5m/s, it was observed that air velocity at 5m/s has the highest amount of cooling as compared to 0.5 m/s. Table 17 shows the change in parameter for air inlet velocity. Figure 19 shows the variations of water temperature along the length of plate for different values of air inlet velocity.

Table 17. Change in inlet parameter for air inlet velocity

Parameters	Values	Units
Height	3	m
Air Velocity inlet	0.5 – 5	m/s
Temperature Air inlet:	30	◦C
Temperature water inlet:	40	◦C
Water flow rate inlet:	0.011	kg/s

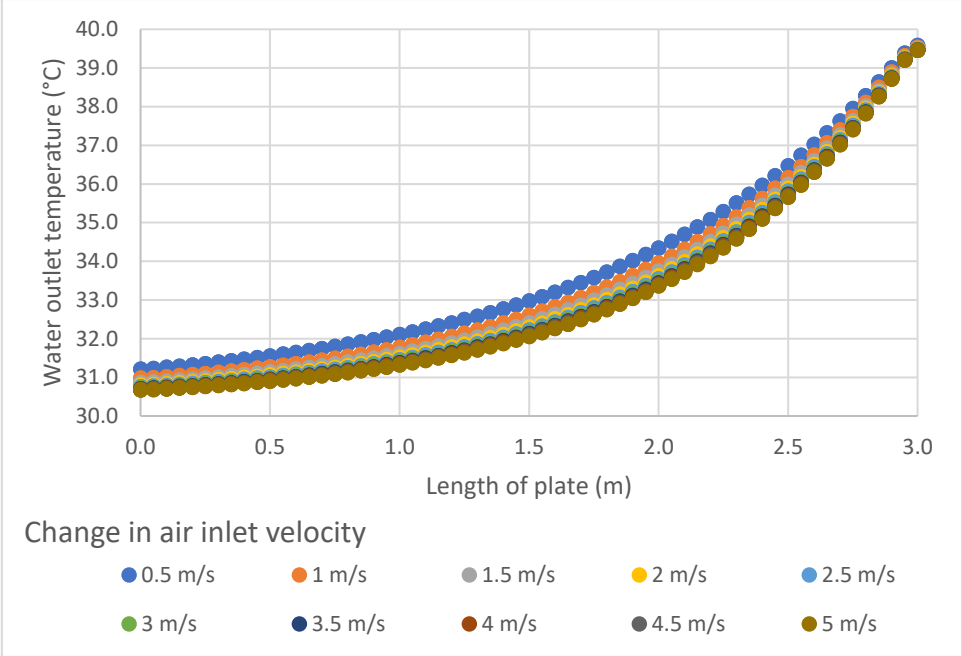

Figure 19. Water temperature along length of plate

12.5 Effects of varying air inlet temperature

When varying air inlet temperature from 18 – 30 ◦C, it was observed that there was no change in water outlet temperature when air inlet temperature was at 18 ◦C and 20 ◦C. The water outlet temperature gradient increases when air inlet temperature decreases. Table 18 shows the change in parameter for air inlet velocity. Figure 20 shows the variations of water temperature along the length of plate for different values of air inlet velocity.

Table 18. Change in inlet parameter for air inlet temperature

Parameters	Values	Units
Height	3	m
Air Velocity inlet	2	m/s
Temperature Air inlet:	18 – 30	◦C
Temperature water inlet:	40	◦C
Water flow rate inlet:	0.011	kg/s

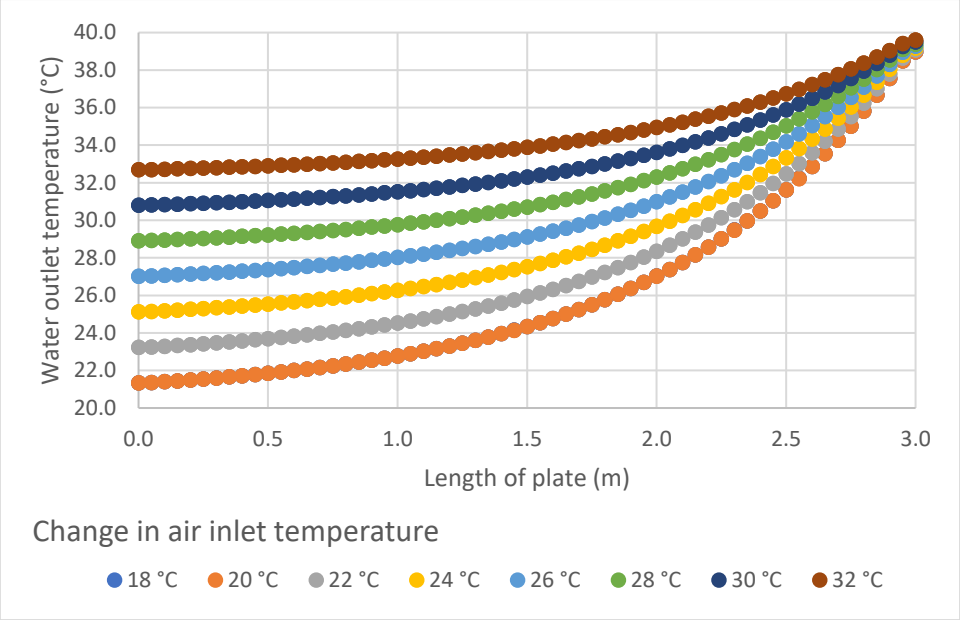

Figure 20. Variation of water temperature along length of plate with differing air inlet temperature

13. Control strategies

After conducting parametric studies on MATLAB and ANSYS (fluent) two control strategies are investigated. The first strategy involves the precooling of ambient air. The cooling of ambient air temperature allows greater heat transfer between ambient air and water when entering the cooling tower. Different configurations of ambient air pre-cooling are investigated to determine the most optimal design [21].

The second strategy is the creation of a neural network function to predict the thermal behaviour of tower. The neural network will help the operator by reducing computational time and effort.

14. Precooling of ambient air

In this section, a simple design of an ambient air cooler is explored to reduce the temperature of ambient air. Simulations will be conducted to analyze and study the system. Figure 21 shows a setup of an ambient air heat exchanger [22].

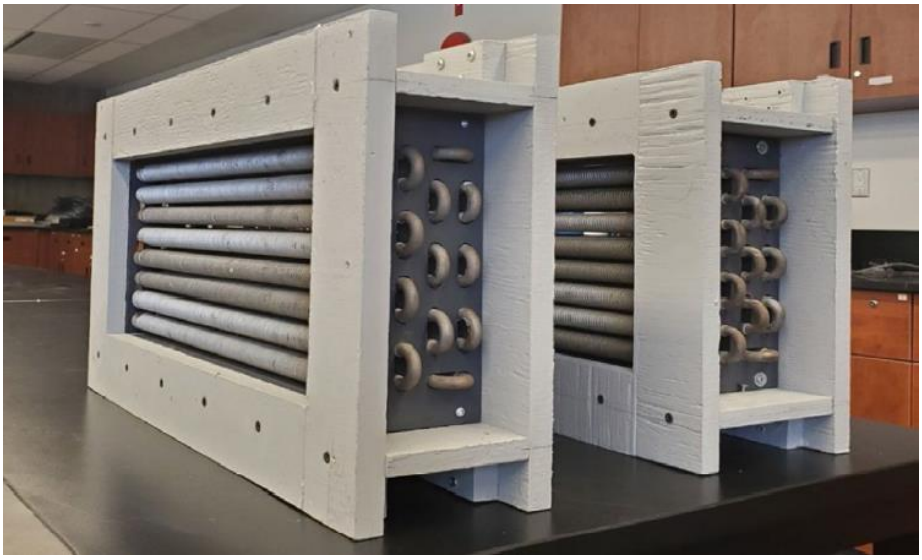

Figure 21. Ambient air heat exchanger

Due to the ANSYS student mesh limit of 512,000 cells/nodes, the setup of the initial design could not be loaded. The design of crossflow configuration was modified by removing pipe bends to reduce the number of nodes and increase the number of pipes for more heat transfer. As mentioned by Abraham, design and inlet parameters were adopted [22]. Figure 22 shows the initial and improved design on ANSYS.

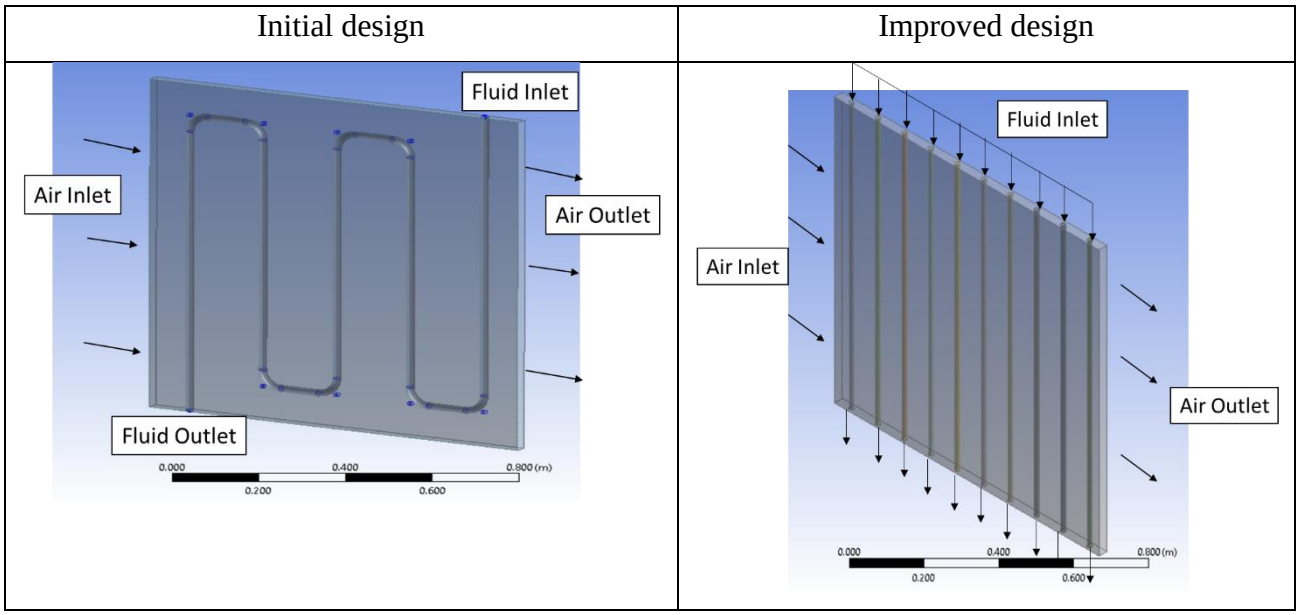

Figure 22. Initial design and improve design 3-D design on ANSYS

14.1 Crossflow configuration with 100mm pipe gap

Table 19 shows the design configurations of a crossflow ambient air pre-cooler.

Table 19. Design configurations of crossflow air pre-cooler

Design Parameters	Value	Units
Length	1	m
Breadth	30	mm
Height	1	m
Diameter of pipe	10	mm
Gap between tubes	100	mm
Fin/non-finned	Non-finned pipe	N. A
Type of pipe configuration	1 shell 10 tube pass	

Figure 23 shows the 3-D design of the design configuration of a crossflow air pre-cooler. Figure 24 shows the boundary condition of the crossflow air pre-cooler.

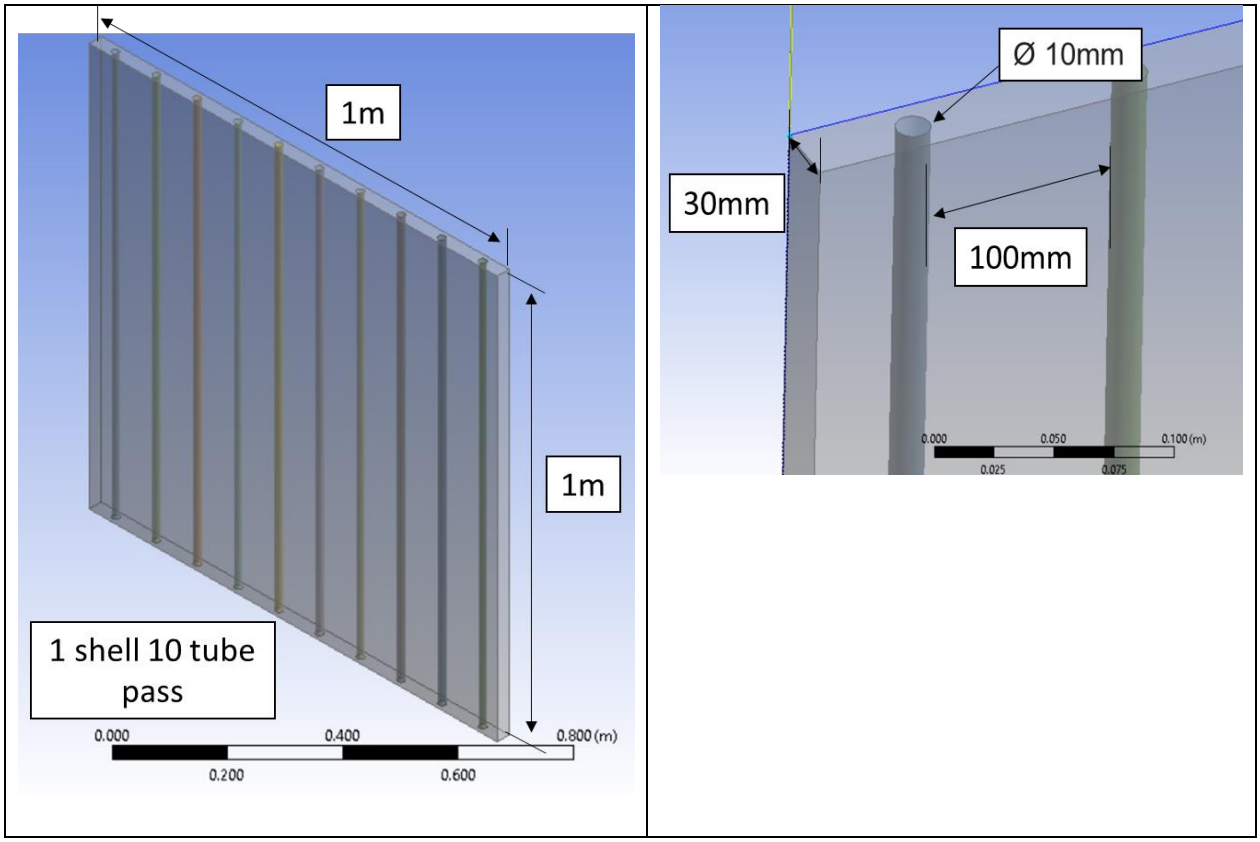

Figure 23. Design of crossflow air pre-cooler

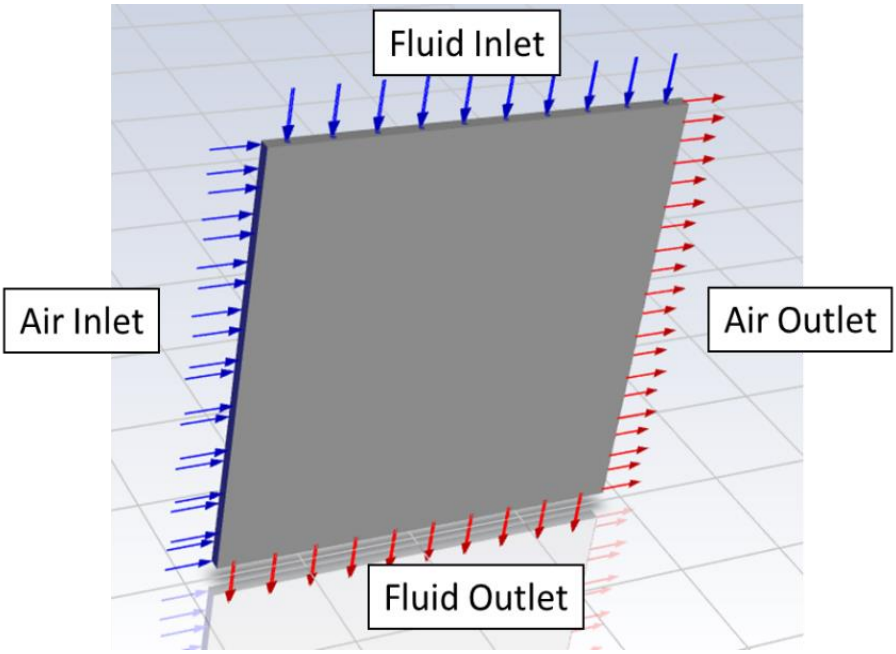

Figure 24. Boundary condition for crossflow air pre-cooler

14.2 Effects of varying water temperature in crossflow configuration

It is observed that the most heat transfer occurs when water temperature was at 28°C. However, heat transfer between air and water pipe is very low. There was a decrease in air temperature of 0.07°C when water is at 28°C while decrease in air temperature was 0.03°C when water is at 30°C. Table 20 shows the change in parameter for water inlet temperature. Figure 25 shows the variations of air temperature along the length of air pre-cooler for different values of water inlet temperature.

Table 20. Change in inlet parameter for water inlet temperature

Parameters	Values	Units
Water Temperature	28 - 30	°C
Air Temperature	32	°C
Water Mass flow rate	0.012	kg/s
Air Velocity	2.75	m/s

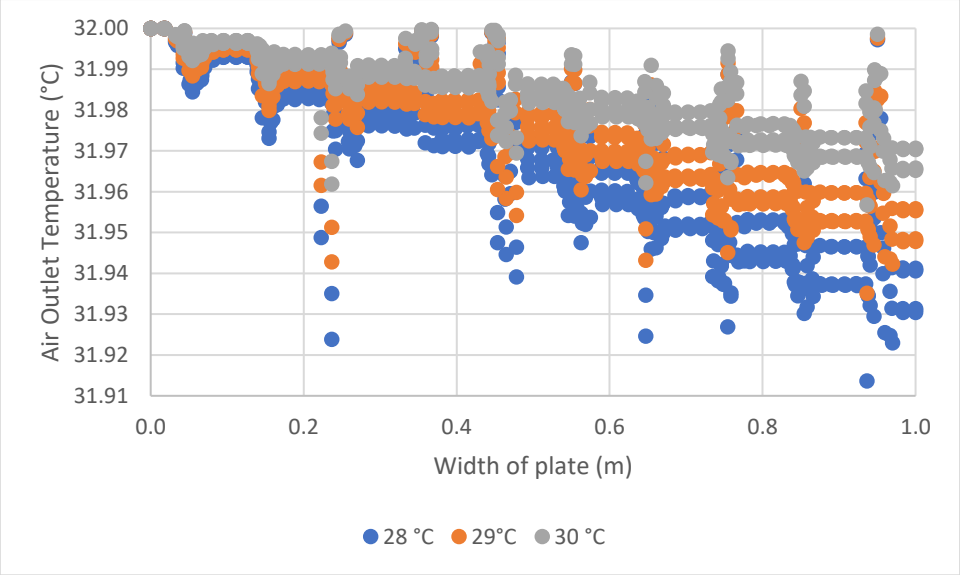

Figure 25. Variation of air temperature along air pre-cooler with differing water inlet temperatures

14.3 Crossflow configuration with 50mm pipe gap

The design of ambient air precooler was modified by reducing the pipe gap to observe if there is an increase in heat transfer between air and water. Table 21 shows the change in design for crossflow pre-cooler. Figure 26 shows the new crossflow heat design with 50mm pipe gaps. The rest of design for pre-cooler was not modified.

Table 21. Design configurations of crossflow air pre-cooler

Design Parameters	Values	Units
Length	0.5	m
Breadth	30	mm
Height	1	m
Diameter of pipe	10	mm
Gap between tubes	50	mm
Fin/non-finned	Non-finned pipe	N. A
Type of pipe configuration	1 shell 10 tube pass	

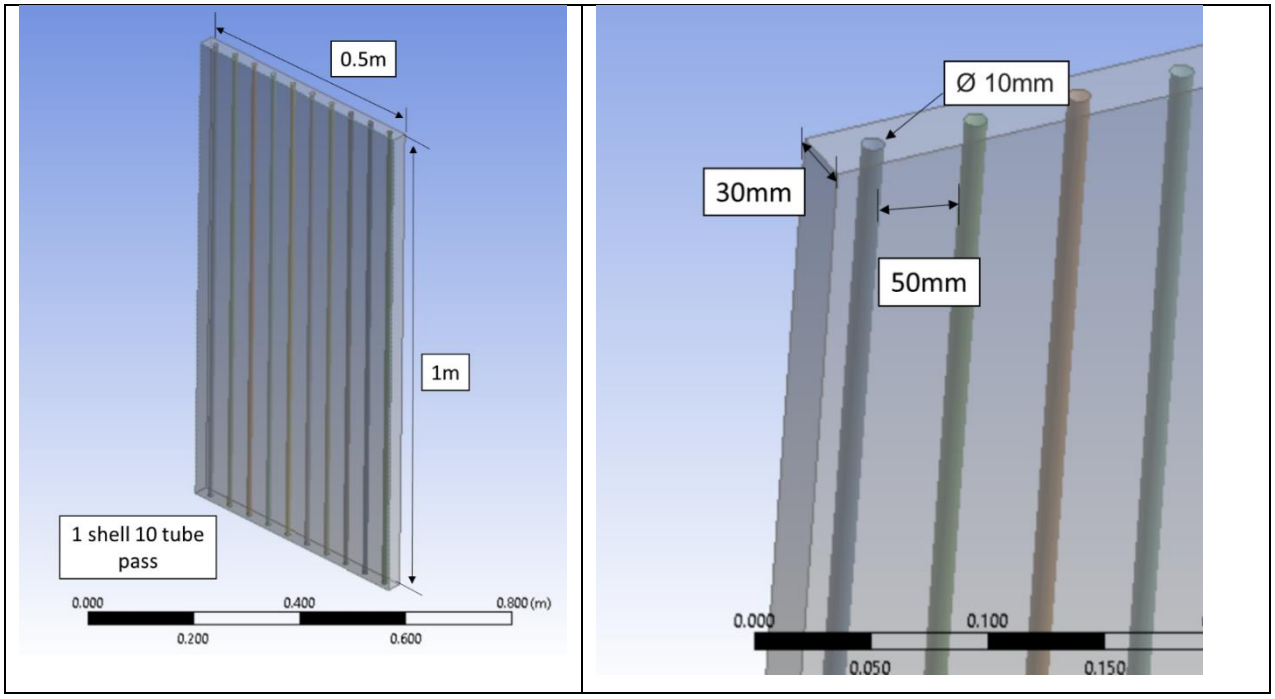

Figure 26. 3-D design of air pre-cooler with 50mm pipe gaps

It was observed that by reducing the pipe gaps, there is no significant decrease in air temperature when air passes through the pipes. Table 22 shows the change in parameter for water inlet temperature. Figure 27 shows the variations of air temperature along the length of air pre-cooler for different values of water inlet temperature.

Table 22. Operating inlet parameter for water inlet temperature

Inlet Parameters	Value	Units
Water Temperature	28 – 30	°C
Air Temperature	32	°C
Water Mass flow rate	0.012	kg/s
Air Velocity	2.75	m/s

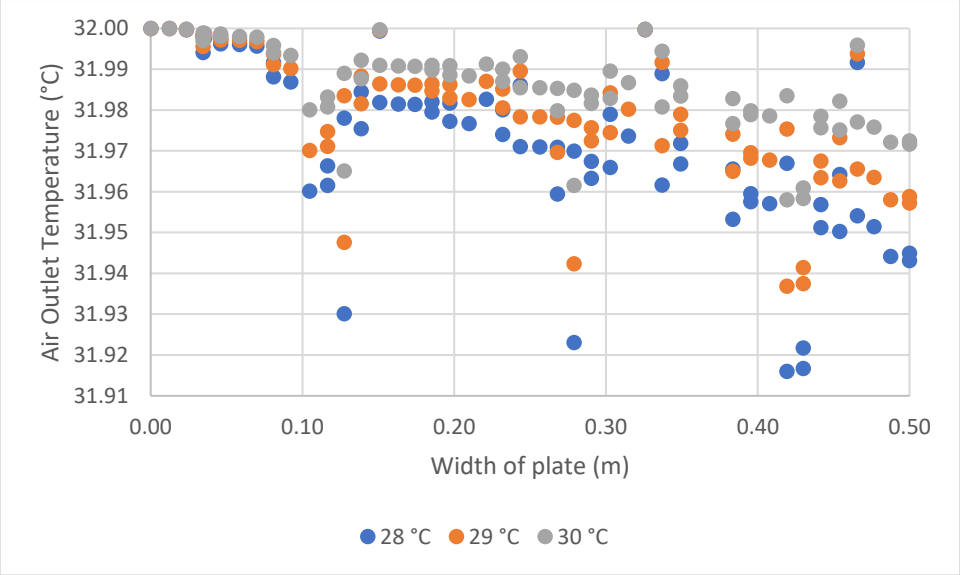

Figure 27. Variation of air temperature along air pre-cooler with differing water inlet temperatures

14.4 Crossflow configuration with 30mm pipe gap

The design of crossflow configuration was further modified with a 30mm pipe gap to observe if there is any improvement of heat transfer between air and water. Table 23 shows the change in design for crossflow pre-cooler. Figure 28 shows the new crossflow heat design with 30mm pipe gaps. The rest of design for pre-cooler was not modified.

Table 23. Design configurations of crossflow air pre-cooler

Design Parameters	Values	Units
Length	0.3	m
Breadth	30	mm
Height	1	m
Diameter of pipe	10	mm
Gap between tubes	30	mm
Fin/non-finned	Non-finned pipe	N. A
Type of pipe configuration	1 shell 10 tube pass	

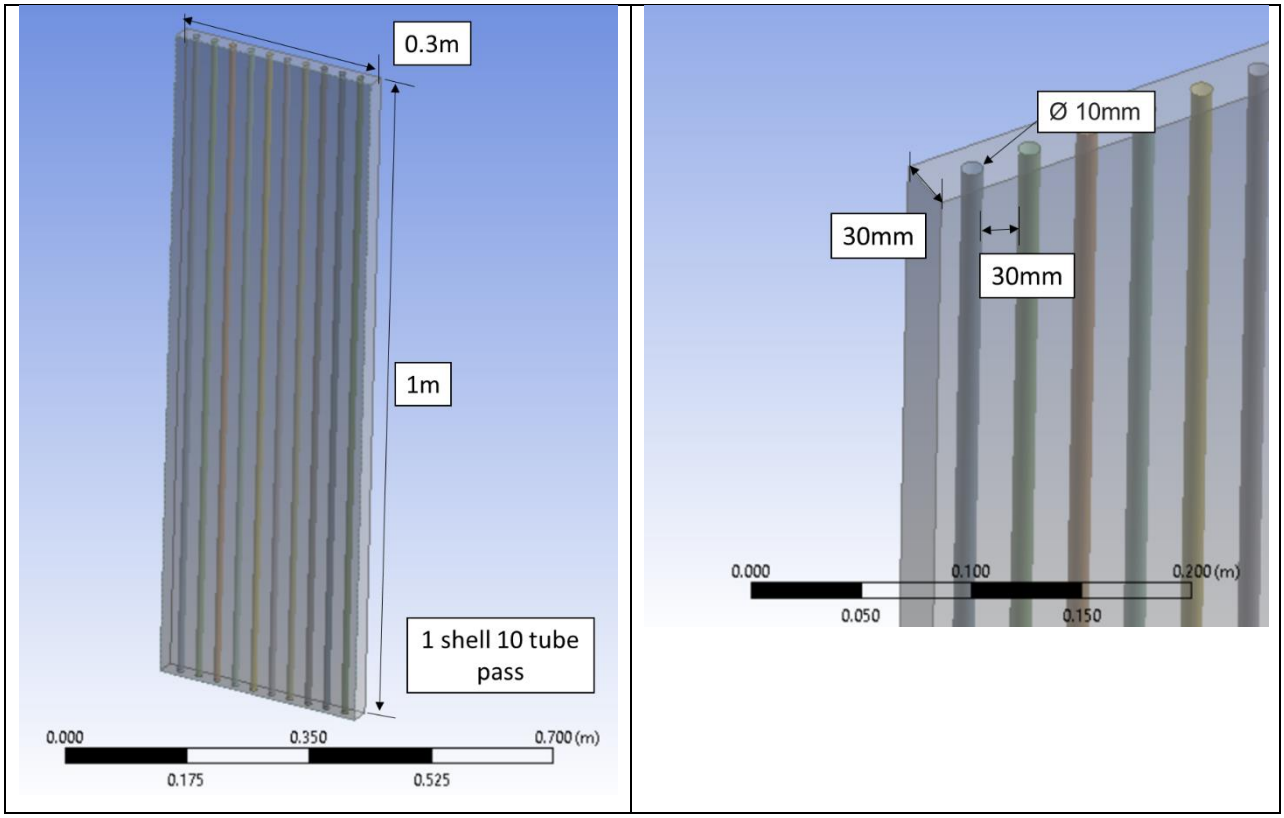

Figure 28. 3-D design of air pre-cooler with 30mm pipe gaps

As seen in air outlet graph presented in Figures 29, varying pipe gaps have little to no cooling effect. Since there is little heat transfer between water and air, counter flow configurations with fins are investigated. Table 23 shows the change in parameter for water inlet temperature. Figure 29 shows the variations of air temperature along the length of air pre-cooler for different values of water inlet temperature.

Table 23. Operating inlet parameters for water inlet temperature

Inlet Parameters	Value	Units
Water Temperature	28 – 30	°C
Air Temperature	32	°C
Water Mass flow rate	0.012	kg/s
Air Velocity	2.75	m/s

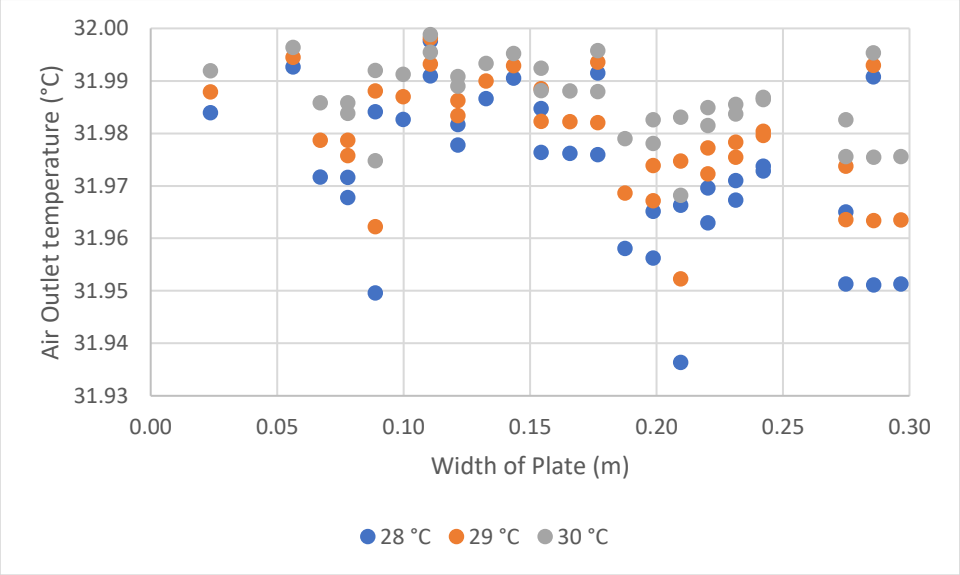

Figure 29. Variation of air temperature along air pre-cooler with differing water inlet temperatures

14.5 Counter-flow configuration with 8 fins

A counter-flow configuration with 8 fins is investigated to observe if there is an increase in heat transfer between air and water. Table 24 shows the design specification for counter-flow air pre-cooler. Figure 30 shows the counter-flow design with 8 fins and boundary conditions.

Table 24. Design specifications for counter-flow configuration with 8 fins

Design Parameters	Value	Units
Length	30	mm
Breadth	30	mm
Height	0.5	m
Diameter of pipe	10	mm
Number of fins	8	N. A
Length of fin	5	mm
Breath of fin	1	mm

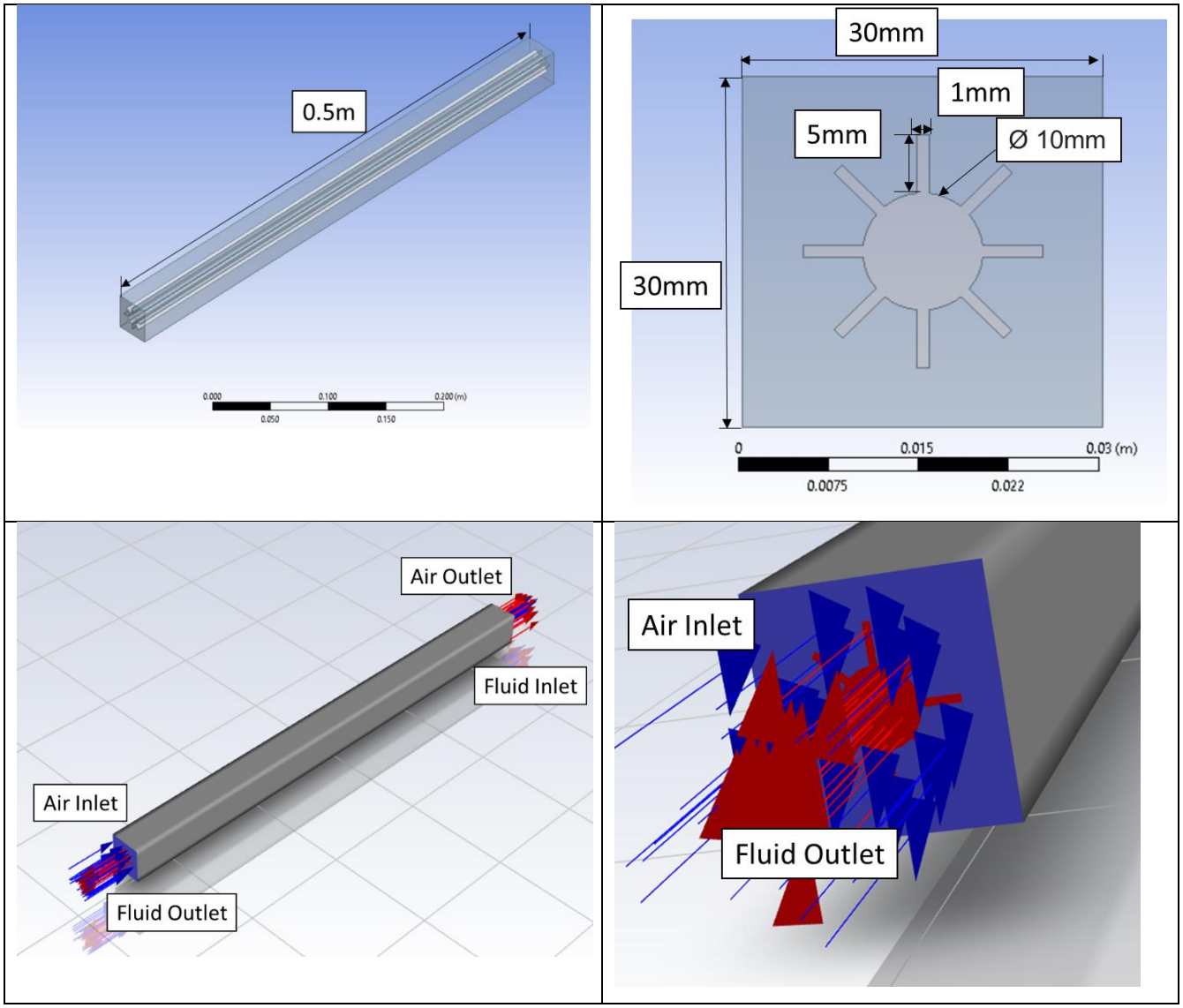

Figure 30. counter-flow design with 8 fins and boundary conditions

To observe if there is an improvement of heat transfer for counter-flow configuration, various water mass flow rate and air velocity are tested. Table 25 shows the change in parameter for water mass flow rate and air velocity.

Table 25. Change in parameter for water mass flow rate and air velocity

Inlet Parameters	Value	Units
Water Temperature	29	°C
Air Temperature	32	°C
Water Mass flow rate	0.010 - 0.015	kg/s
Air Velocity	1.75 – 4.5	m/s

14.5.1 Change in air velocity

There are two curve graphs in each data as ANSYS collects two readings for the air domain when running the simulation. Hence, should specific calculation involve in final temperature of air, the median value of the two-curve graph is taken as final value. As observed in table 30, air inlet velocity at 1.75m/s have the highest cooling effect as compared to the other velocities. However, the drop in temperature is still insignificant, 0.3 °C. Figure 31 shows the variations of air temperature along the length of air pre-cooler for different values of air inlet velocity.

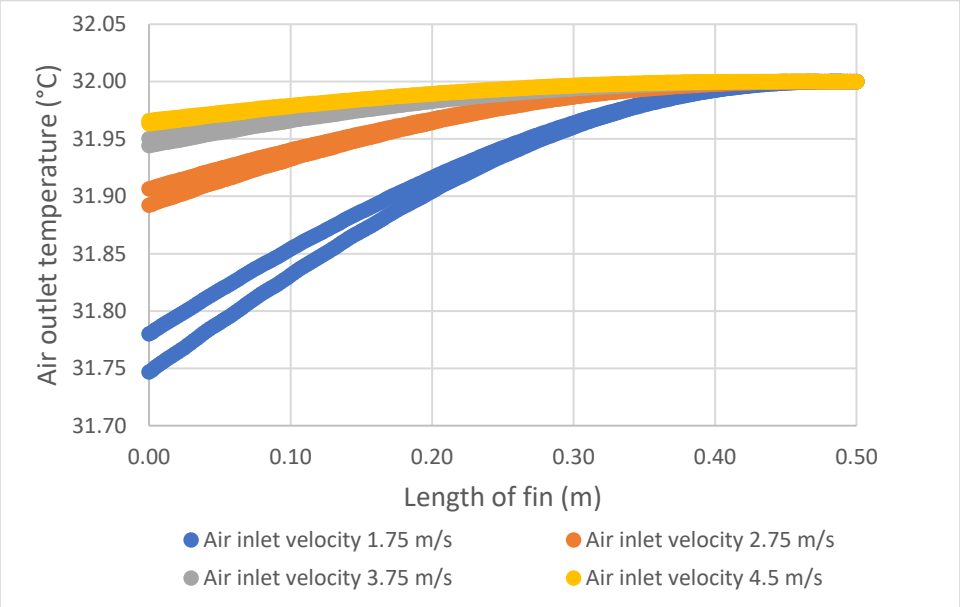

Figure 31. Variation of air temperature along air pre-cooler with differing air inlet velocities

14.5.2 Change in water flow rate

There are two curve graphs in each data as ANSYS collects two readings for the air domain when running the simulation. Hence, should specific calculation involve in final temperature of air, the median value of the two-curve graph is taken as final value. It is observed that when water flow rate is increased, there not a significant increase in cooling. Figure 32 shows the variations of air temperature along the length of air pre-cooler for different values of water inlet mass flow rate.

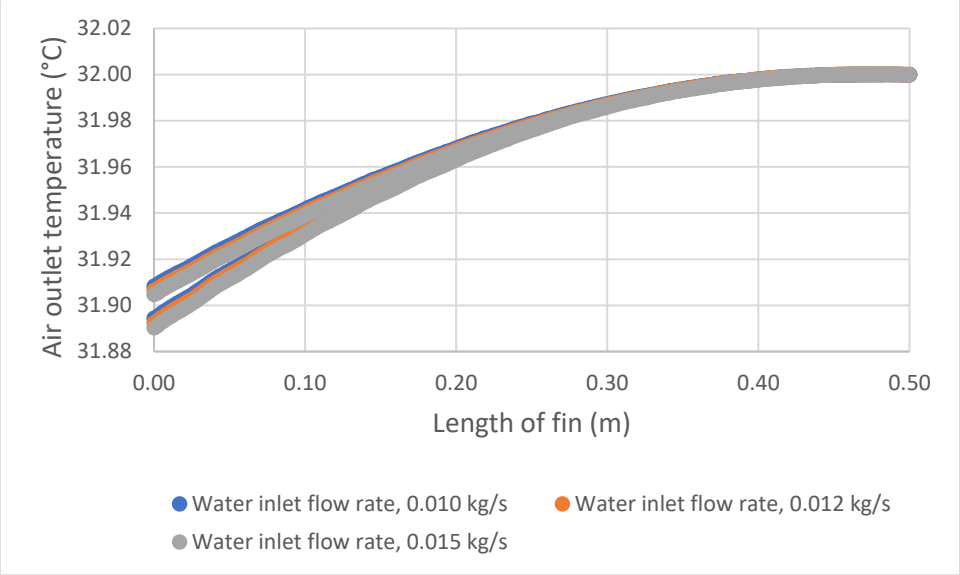

Figure 32. Variation of air temperature along air pre-cooler with differing water flow rates

14.6 Counter-flow configuration with 16 fins

A counter-flow configuration with 16 is investigated to observe it there is an increase in cooling effect when number of fins are increased from 8 to 16 fins. Table 26 shows the design specification for counter-flow air pre-cooler. Figure 33 shows the counter-flow design with 16 fins.

Table 26. Design specifications for counter-flow configuration with 16 fins

Design Parameters	Value	Units
Length	30	mm
Breadth	30	mm
Height	0.5	m
Diameter of pipe	10	mm
Number of fins	16	N. A
Length of fin	5	mm
Breath of fin	1	mm

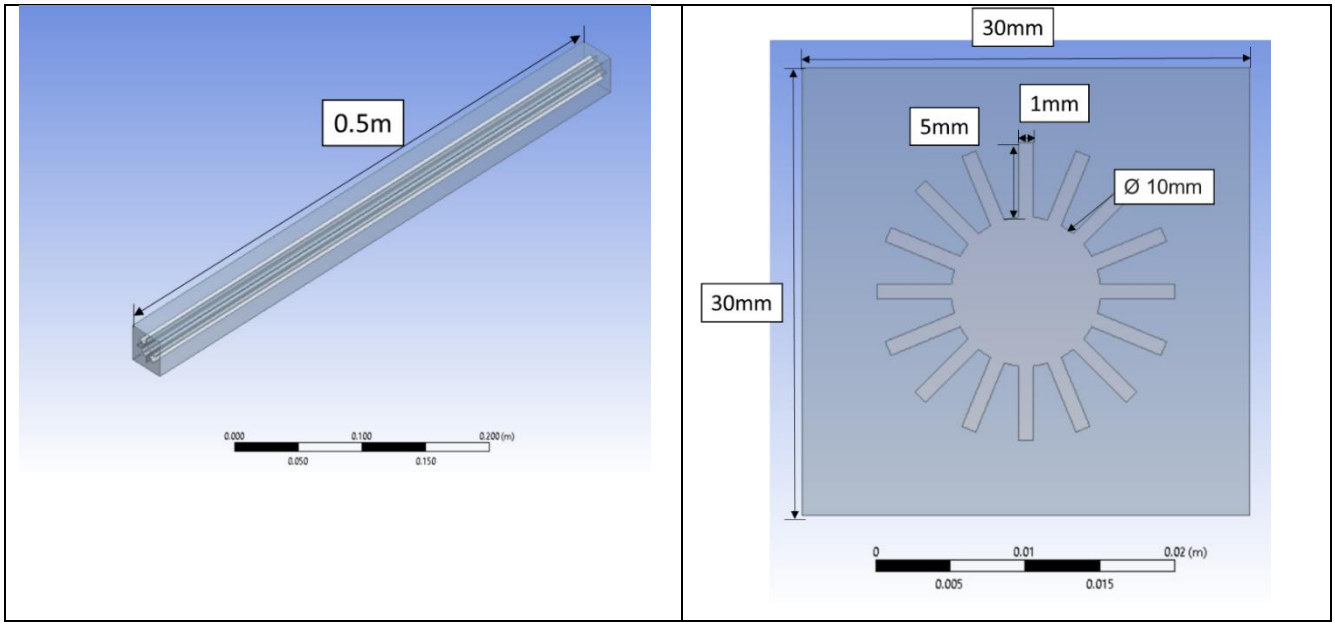

Figure 33. Design of counter-flow air heat exchanger, 16 finned tube

To observe if there is an improvement of heat transfer for counter-flow configuration from 8 fins to 16 fins, various water mass flow rate and air velocity are tested. Table 27 shows the change in parameter for water mass flow rate and air velocity.

Table 27. Change in parameter for water mass flow rate and air velocity

Inlet Parameters	Value	Units
Water Temperature	29	°C
Air Temperature	32	°C
Water Mass flow rate	0.010 – 0.015	kg/s
Air Velocity	1.75 – 4.5	m/s

14.6.1 Change in air velocity

There are two curve graphs in each data as ANSYS collects two readings for the air domain when running the simulation. Hence, should specific calculation involve in final temperature of air, the median value of the two-curve graph is taken as final value. For the 16 fins configuration, it is observed that when air velocity at 1.75 m/s, it has the highest cooling of 1°C. Figure 34 shows the variations of air temperature along the length of air pre-cooler for different values of air inlet velocity.

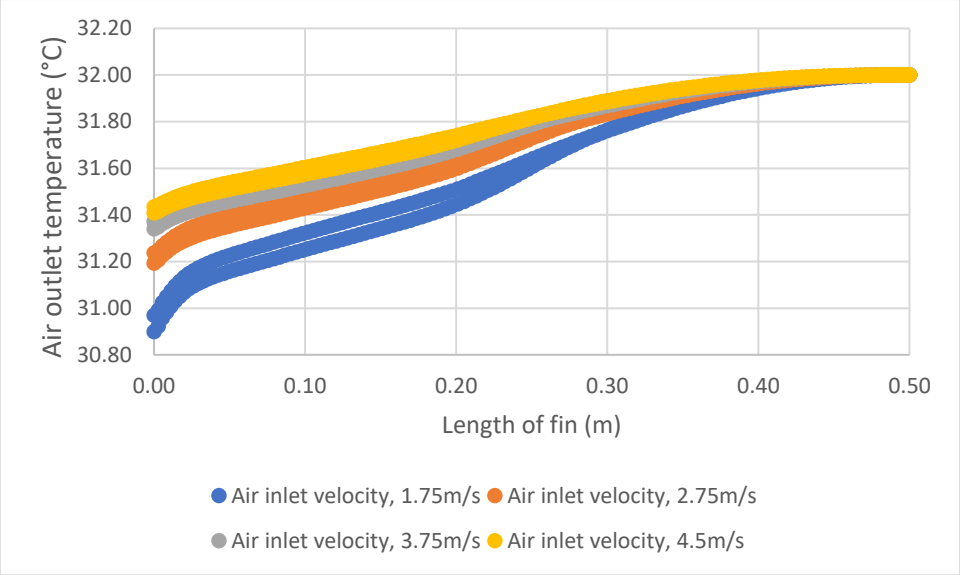

Figure 34. Variation of air temperature along air pre-cooler with differing air inlet velocities

14.6.2 Change in water flow rate

There are two curve graphs in each data as ANSYS collects two readings for the air domain when running the simulation. Hence, should specific calculation involve in final temperature of air, the median value of the two-curve graph is taken as final value. It is observed that when the water flow rate is the highest at 0.015kg/s, it has the highest cooling of 1°C. Figure 35 shows the variations of air temperature along the length of air pre-cooler for different values of water inlet mass flow rate.

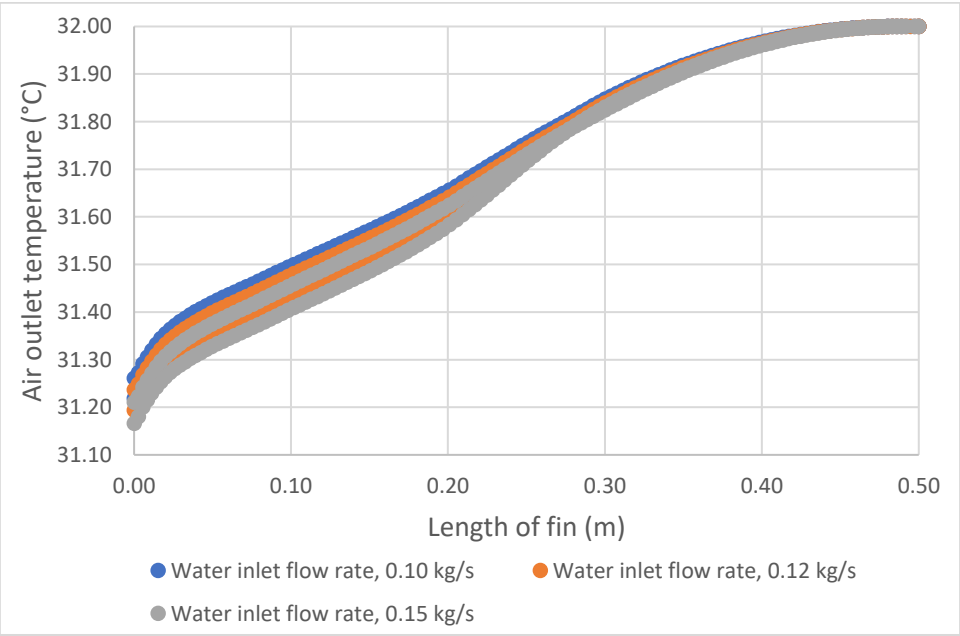

Figure 35. Variation of air temperature along air pre-cooler with differing water flow rates

From the studies conducted, counterflow configuration with fins provides a higher cooling effect as compared to crossflow configuration. However, counterflow configuration with 16 fins provided a better cooling effect in comparison to 8 fins as it has more surface area for heat transfer between water and air. Figure 36 shows an air temperature volume rendering of the model when air velocity is at 1.7 m/s. Figure 37 shows an air temperature volume rendering of the model when water flow rate is at 0.015kg/s.

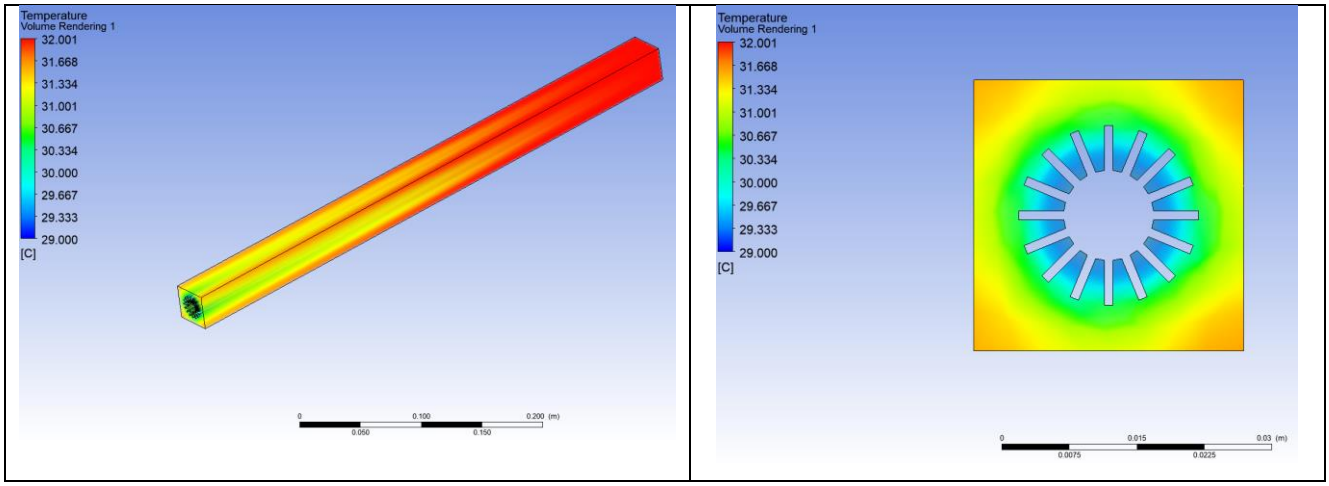

Figure 36. Air temperature volume rendering when air velocity at 1.7m/s

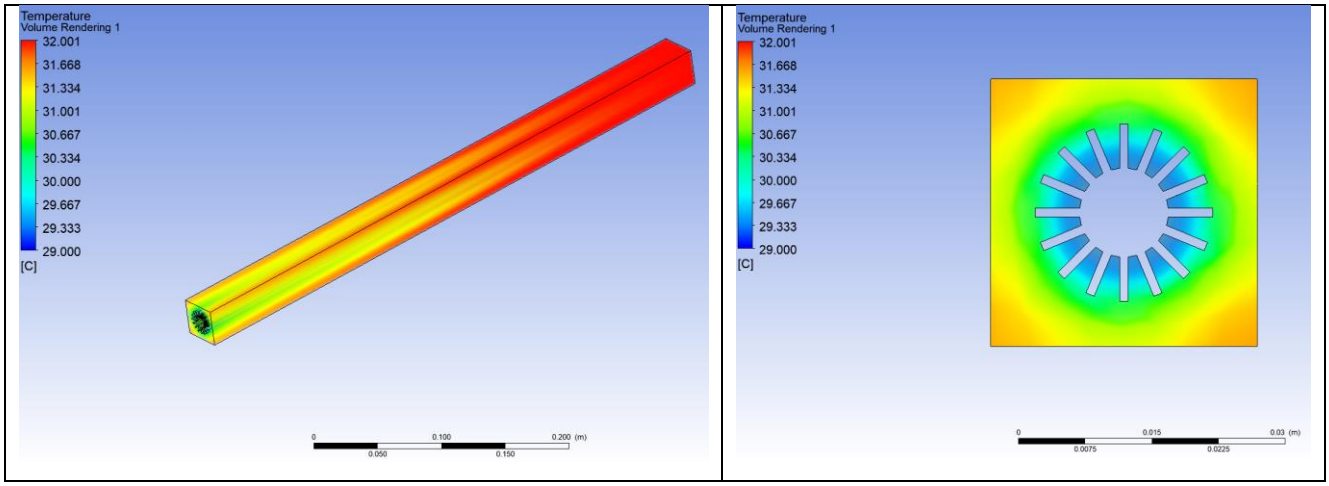

Figure 37. Air temperature volume rendering when water flow rate at 0.015kg/s

14.7 Improvement of counter-flow 8 fin configuration

To further improve the cooling performance of the counterflow finned configuration, the dimensions of the tube and fins are kept constant while the casing of the tube is reduced by 5mm. while 8 and 16 fin configurations are investigated. Table 37 shows the new design

specification for counter-flow air pre-cooler. Figure 38 shows the new counter-flow design with 8 fins.

Table 37. Design specifications for counter-flow configuration with smaller casing

Design Parameters	Value	Units
Length	25	mm
Breadth	25	mm
Height	0.5	m
Diameter of pipe	10	mm
Number of fins	8	
Length of fin	5	mm
Breath of fin	1	mm

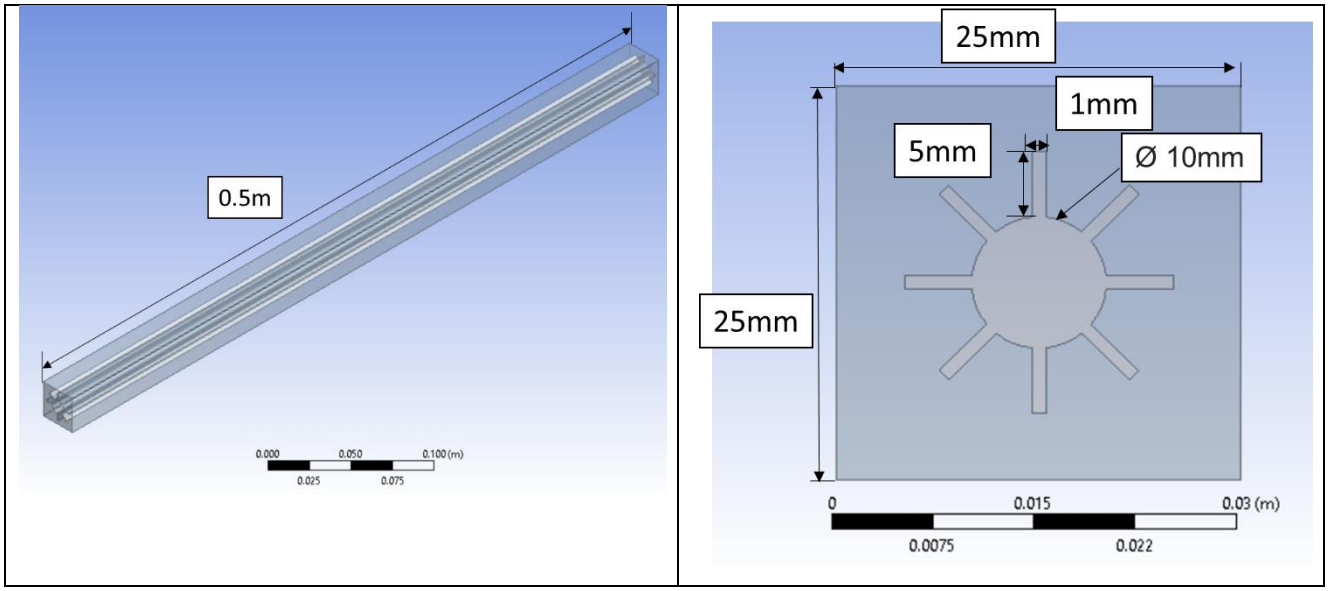

Figure 38. 3-D design of counter-flow air heat exchanger

To investigate if there is an improvement of heat transfer for counter-flow configuration by reducing the casing size, various water mass flow rate and air velocity are tested. Table 38 shows the change in parameter for water mass flow rate and air velocity.

Table 38. Change in parameter for water mass flow rate and air velocity

Inlet Parameters	Value	Units
Water Temperature	29	°C
Air Temperature	32	°C
Water Mass flow rate	0.010 - 0.015	kg/s
Air Velocity	1.75 – 4.5	m/s

14.7.1 Change in air velocity

There are two curve graphs in each data as ANSYS collects two readings for the air domain when running the simulation. Hence, should specific calculation involve in final temperature of air, the median value of the two-curve graph is taken as final value. For the 16 fins configuration, it is observed that when air velocity at 1.75 m/s, it has the highest cooling of 1°C. Figure 39 shows the variations of air temperature along the length of air pre-cooler for different values of air inlet velocity.

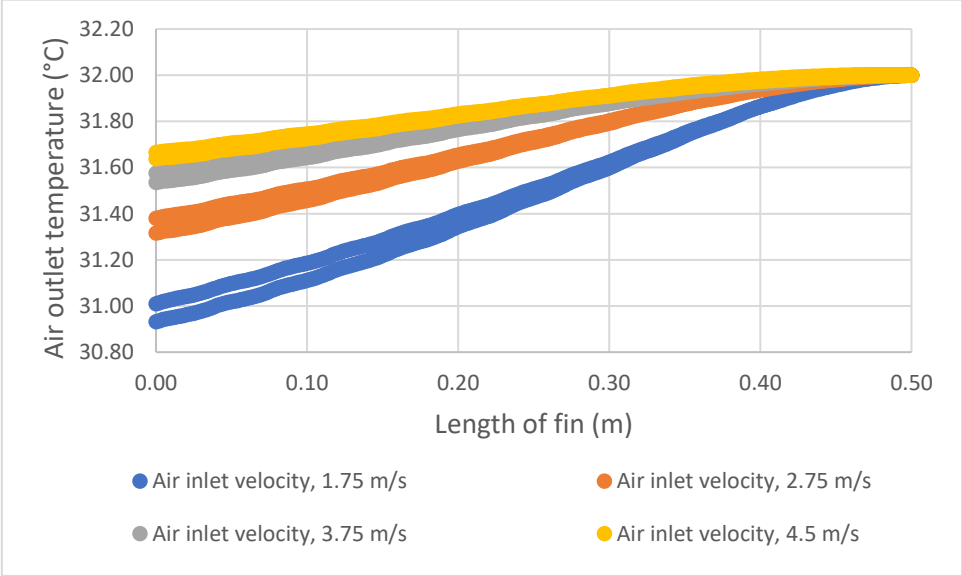

Figure 39. Variation of air temperature along air pre-cooler with differing air inlet velocities

14.7.2 Change in water mass flow rate

There are two curve graphs in each data as ANSYS collects two readings for the air domain when running the simulation. Hence, should specific calculation involve in final temperature of air, the median value of the two-curve graph is taken as final value. It is observed that all presented flow rates have a consistent cooling around 0.65°C. Figure 40 shows the variations

of air temperature along the length of air pre-cooler for different values of water inlet mass flow rate.

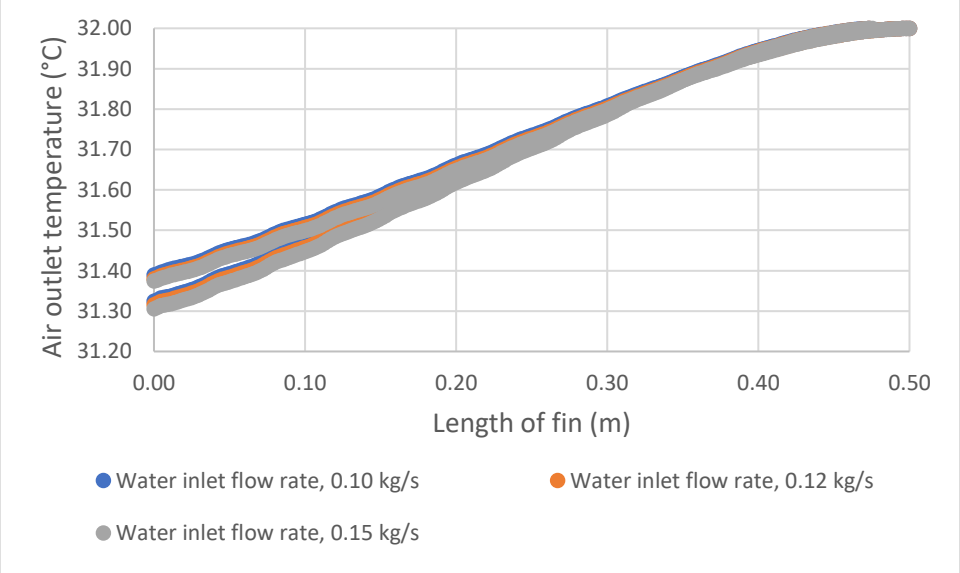

Figure 40. Variation of air temperature along air pre-cooler with differing water flow rates

14.8 Improvement of counter-flow 16 fins configuration

A counter-flow configuration with 16 is investigated to observe it there is an increase in cooling effect when casing size of counter-flow configuration with 16 fin is reduced. Table 39 shows the design specification for counter-flow air pre-cooler. Figure 41 shows the improved counter-flow design with 16 fins.

Table 39. Design specifications for counter-flow configuration with smaller casing

Design Parameters	Value	Units
Length	25	mm
Breadth	25	mm
Height	0.5	m
Diameter of pipe	10	mm
Number of fins	16	N.A
Length of fin	5	mm
Breath of fin	1	mm

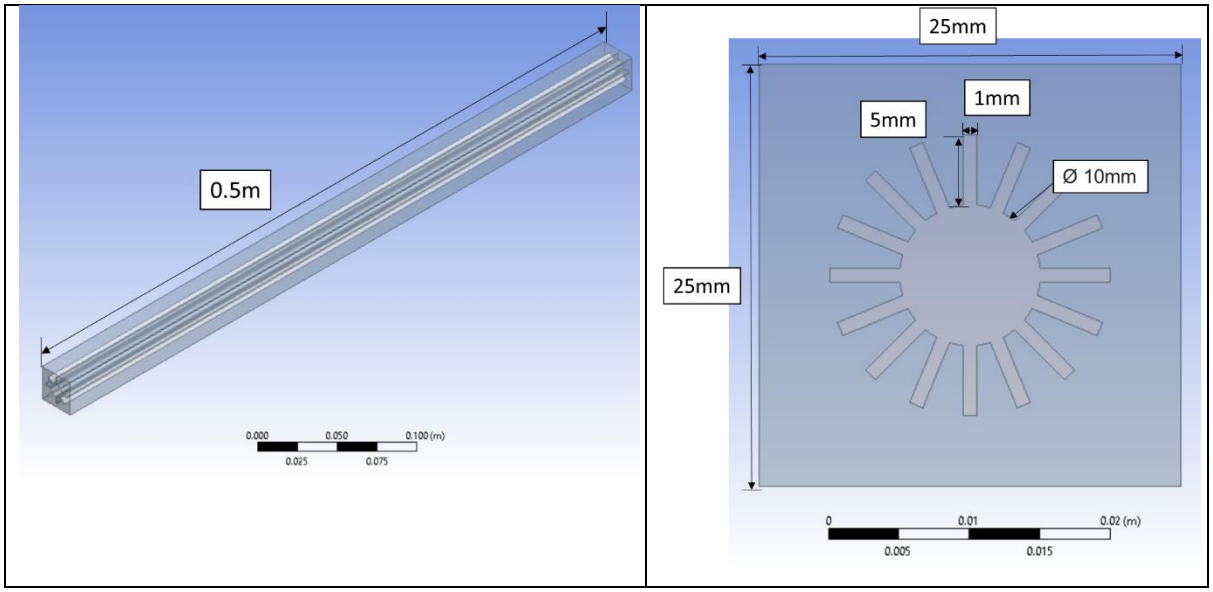

Figure 41. 3-D design of counter-flow air heat exchanger

To investigate if there is an improvement of heat transfer for counter-flow configuration by reducing the casing size, various water mass flow rate and air velocity are tested. Table 40 shows the change in parameter for water mass flow rate and air velocity.

Table 40. Change in parameter for water mass flow rate and air velocity

Inlet Parameters	Value	Units
Water Temperature	29	°C
Air Temperature	32	°C
Water Mass flow rate	0.010 - 0.015	kg/s
Air Velocity	1.75 – 4.5	m/s

14.8.1 Change in air velocity

It is observed that when air velocity at 1.75 m/s, it has the highest cooling of more than 2°C. Figure 42 shows the variations of air temperature along the length of air pre-cooler for different values of air inlet velocity.

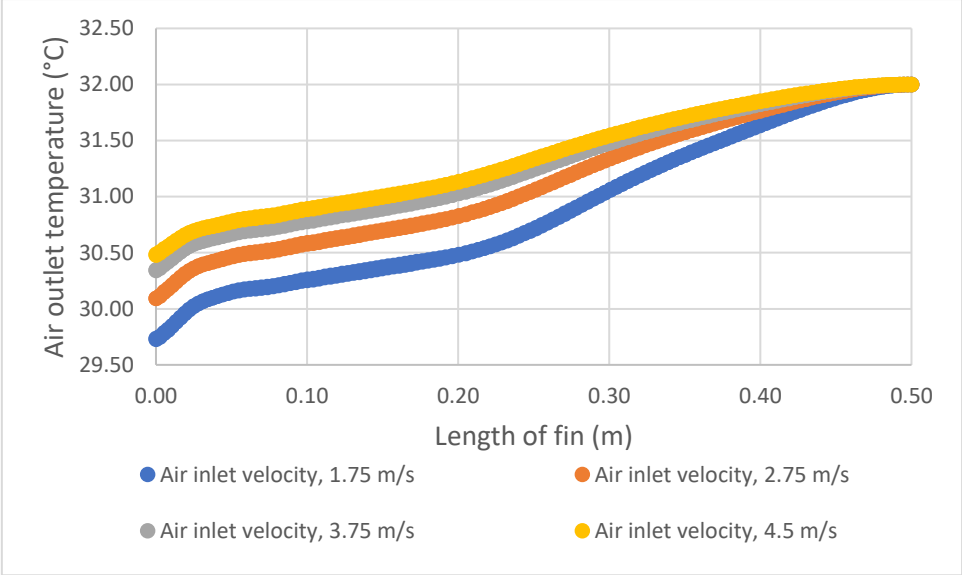

Figure 42. Variation of air temperature along air pre-cooler with differing air inlet velocities

14.8.2 Change in water mass flow rate

It is observed that all presented flow rates have a consistent cooling of 2°C. Figure 43 shows the variations of air temperature along the length of air pre-cooler for different values of water inlet mass flow rate.

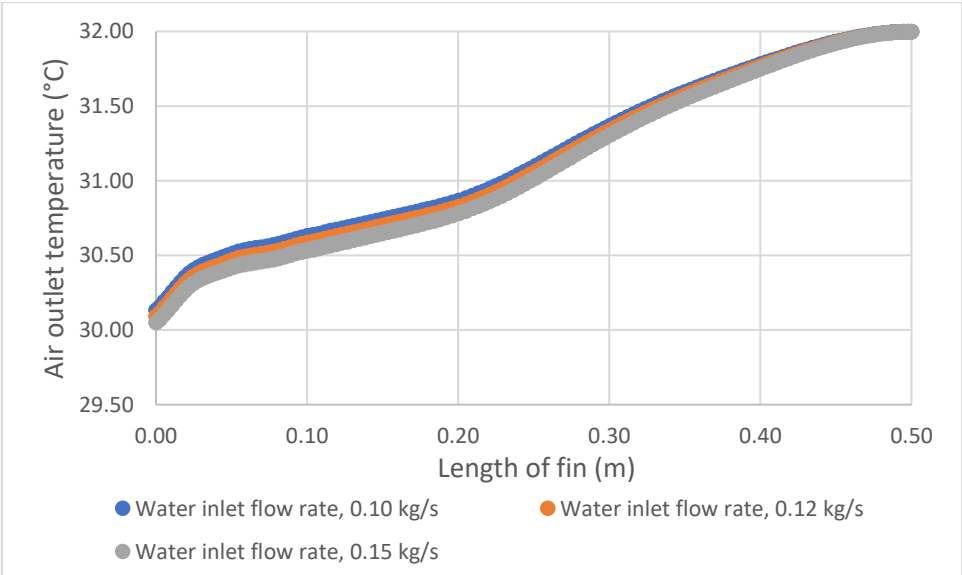

Figure 43. Variation of air temperature along air pre-cooler with differing water flow rates

By reducing the length and breadth by 5mm, the cooling effect was increased by 1 °C. From the graphs, the greatest cooling effect is achieved when air velocity is at 1.75 m/s while the water flow rate is at 0.015kg/s. Figure 44 shows an air temperature volume rendering of the

model when air velocity is at 1.7 m/s. Figure 45 shows an air temperature volume rendering of the model when water flow rate is at 0.015kg/s.

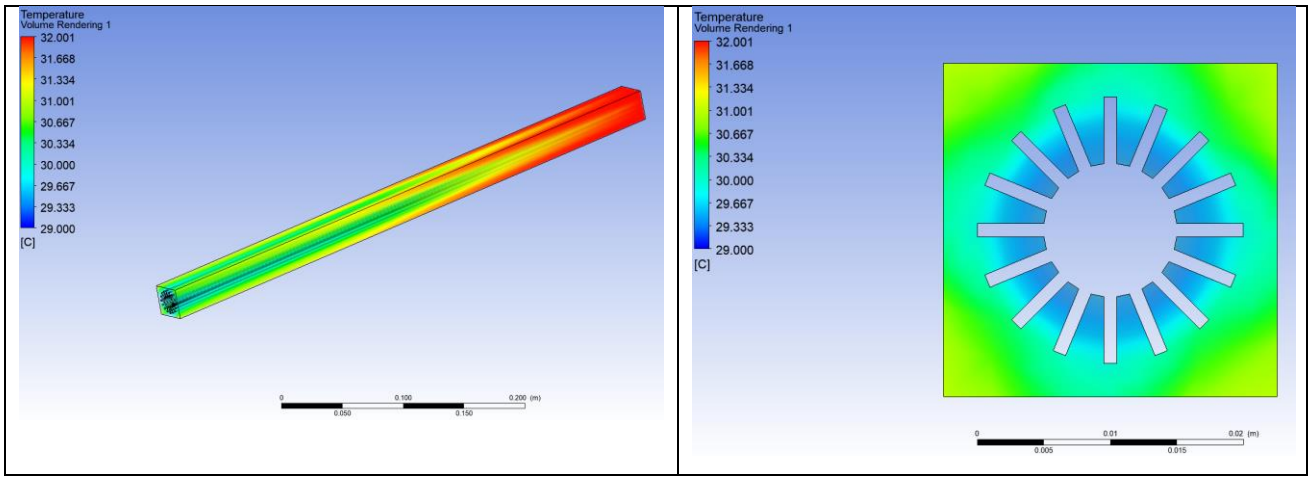

Figure 44. Air temperature volume rendering when air velocity at 1.7m/s

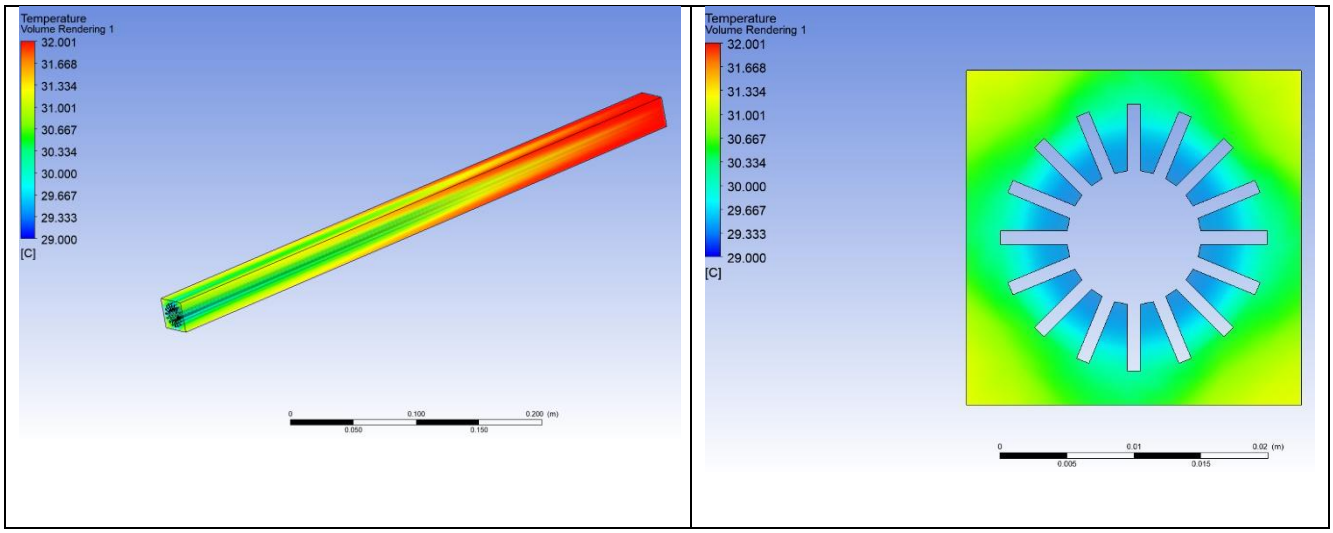

Figure 45. Air temperature volume rendering when water flow rate at 0.015kg/s

After conducting various investigations for pre-cooling of air configurations, a counter-flow configuration, 25mm by 25mm with 16 finned tubes is the best choice for configuration for cooling of ambient air.

15. Neural network prediction for cooling tower performance

In a study conducted by Elsaid, the suggested range for inlet air velocity varied from 0.5 – 2.25m/s. while fluid velocity inlet ranges from 0.05 – 0.17kg/s [6]. This thesis will be adopting the velocity and mass flow rate ranges suggested by published literature while the temperature will be following typical weather and operating conditions in Singapore. The range and list of data collected on MATLAB can be found in appendix. The MATLAB program has been modified to display sensible, latent, and a 100*10 grid graph for visual representation. Table 41 shows MATLAB simulation for inlet operating parameters in typical operating conditions. Figures 46 – 51 shows the MATLAB outlet graphs for temperature gradient of air, temperature gradient of water, latent heat flux, sensible heat flux, evaporation, and relative humidity. The blue arrow represents water inlet and outlet, and the brown arrows represent air inlet and outlet. Figure 46.1 shows a schematic for an illustration of the grid points in the improved MATLAB model.

Table 41. Operating inlet conditions

Inlet Parameters	Value	Unit
T_{wi}	35	°C
Ta_i	30	°C
mf	0.018	°C
RH	70	%
V_{ai}	2.75	m/s
$\dot{m}_{wi}$	0.01360	kg/s

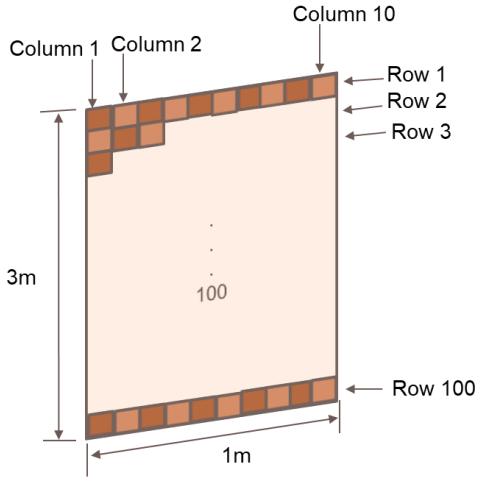

Figure 46.1. Illustration for 100*10 grid point

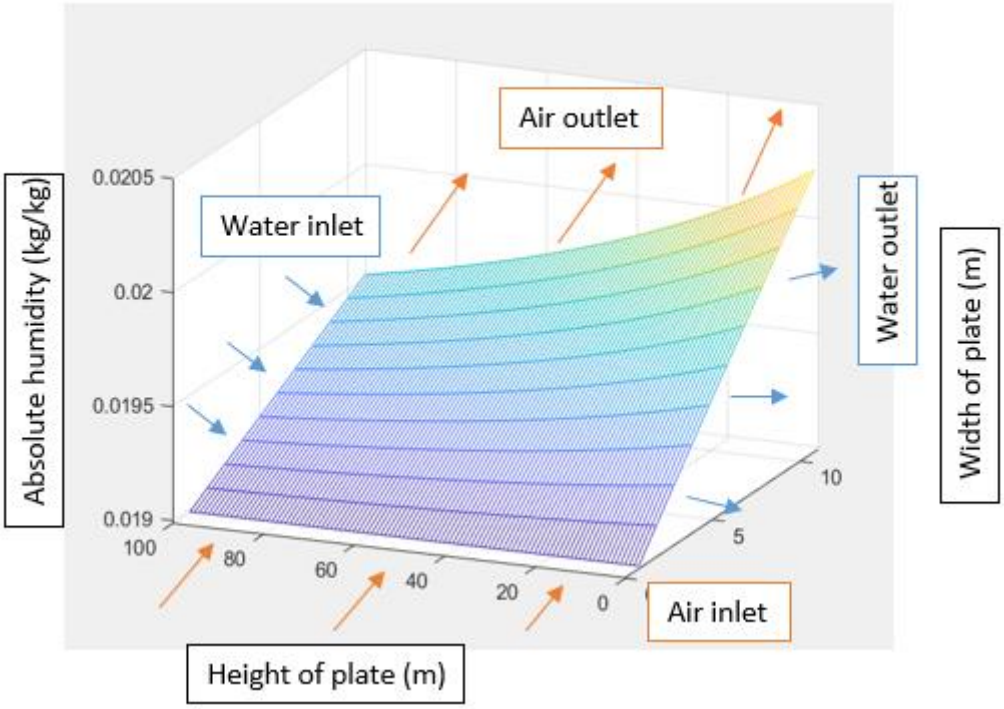

Figure 46. Absolute humidity gradient graph

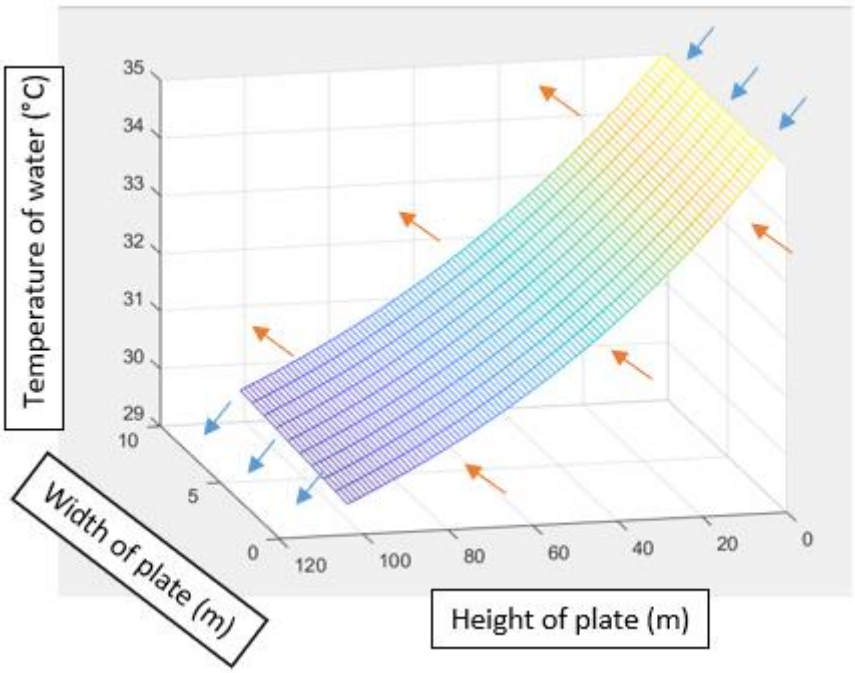

Figure 47. Temperature gradient water graph

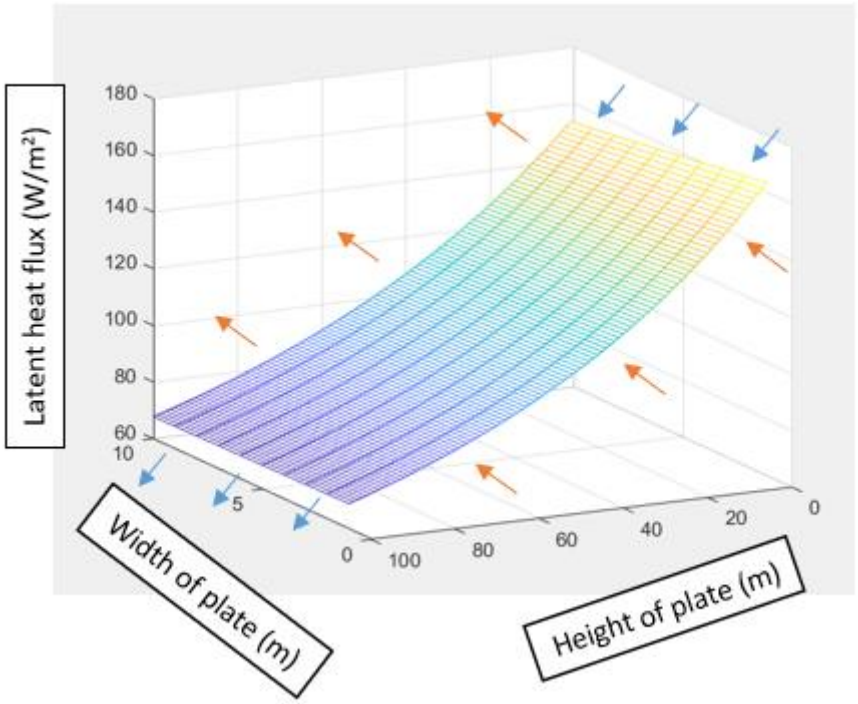

Figure 48. Latent heat flux gradient graph

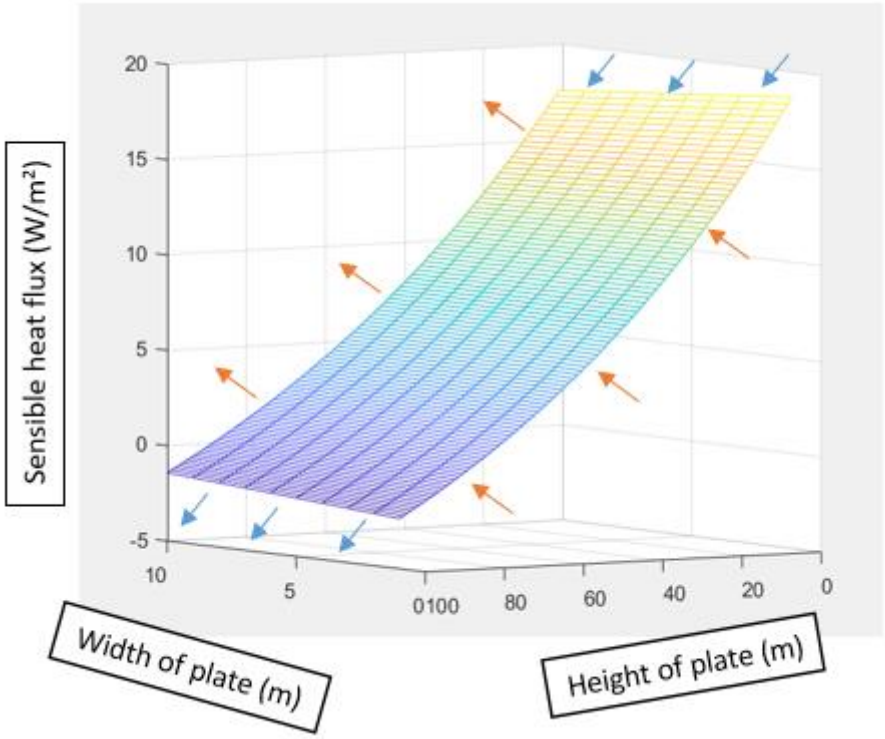

Figure 49. Sensible heat flux gradient graph

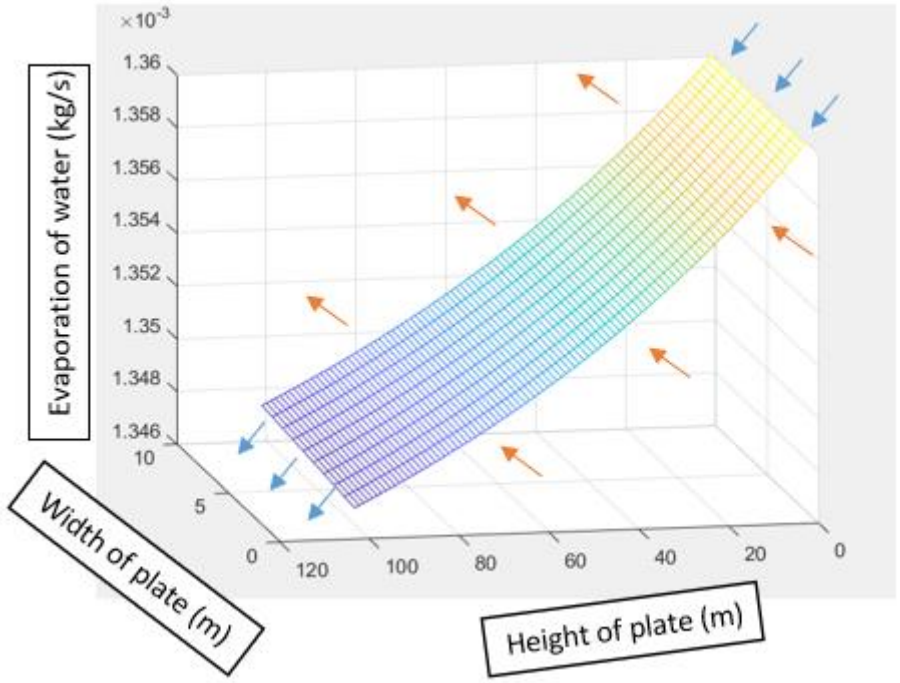

Figure 50. Evaporation gradient graph

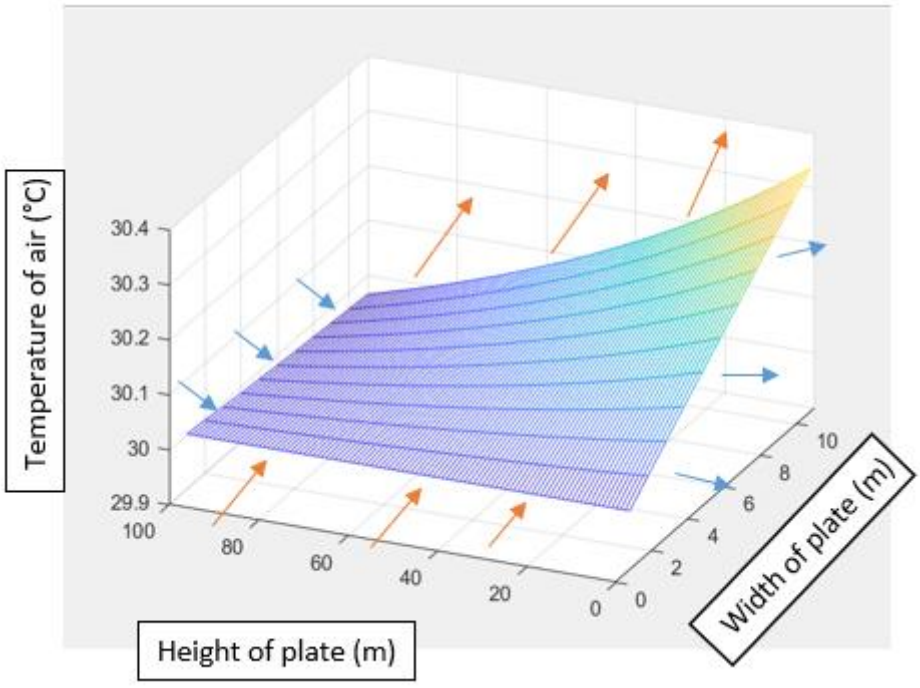

Figure 51. Temperature air gradient graph

The inlet and outlet data collected are used as inlet and target data for the training of neural networks on MATLAB.

15.1 Neural network set up (MATLAB)

The input-output and curve-fitting option were selected on MATLAB as it is the most applicable option. 300 hidden neurons are selected as it provides the best results for training a neural network. The training algorithm, Bayesian Regularization was selected as it provides good generalization for small, noisy, and difficult datasets. A total of 55 datasets were collected for the neural network dataset. Figure 52 shows the schematic of neural network.

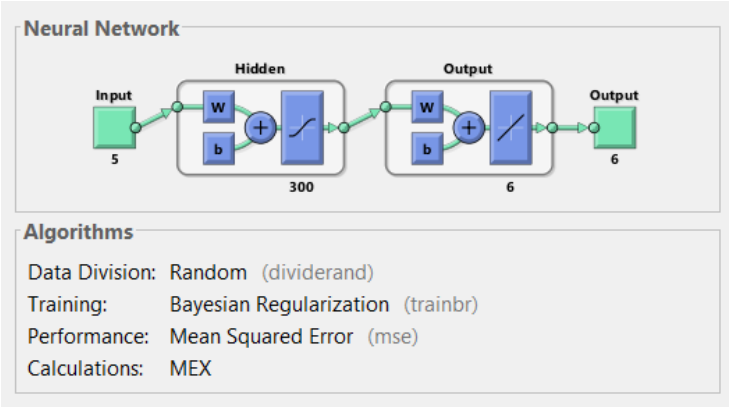

Figure 52. Neural Network

As seen in Figure 53, the regression R measures the correlation between outputs of the neural network and target data provided to MATLAB. An R-value of 1 means a close relationship while an R-value of 0 means a random relationship. As the R values for all three graphs are close to 1, the relationship between target and output data is close. Figure 53 depicts the neural network training regression graph.

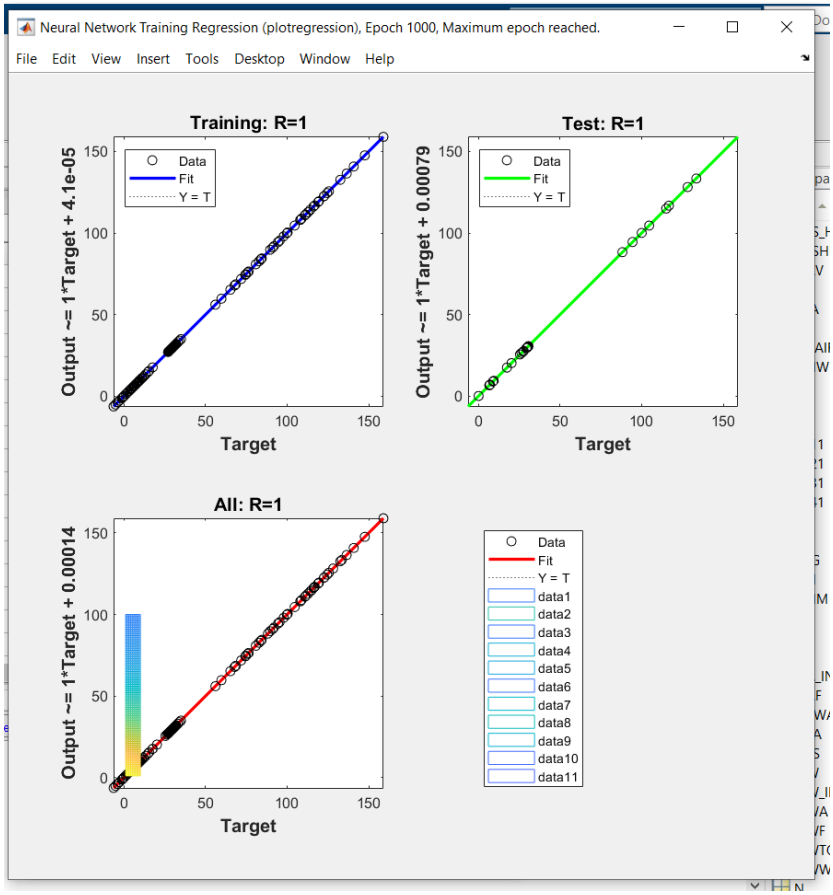

Figure 53. Neural network training regression graph

From Figure 54, the mean squared error is the average difference between outputs and targets. When the value for mean squared error is 0, it means that there is no error. As the data for the train is close to 0, this means that there is little error. Figure 54 shows the mean square error graph for neural network training.

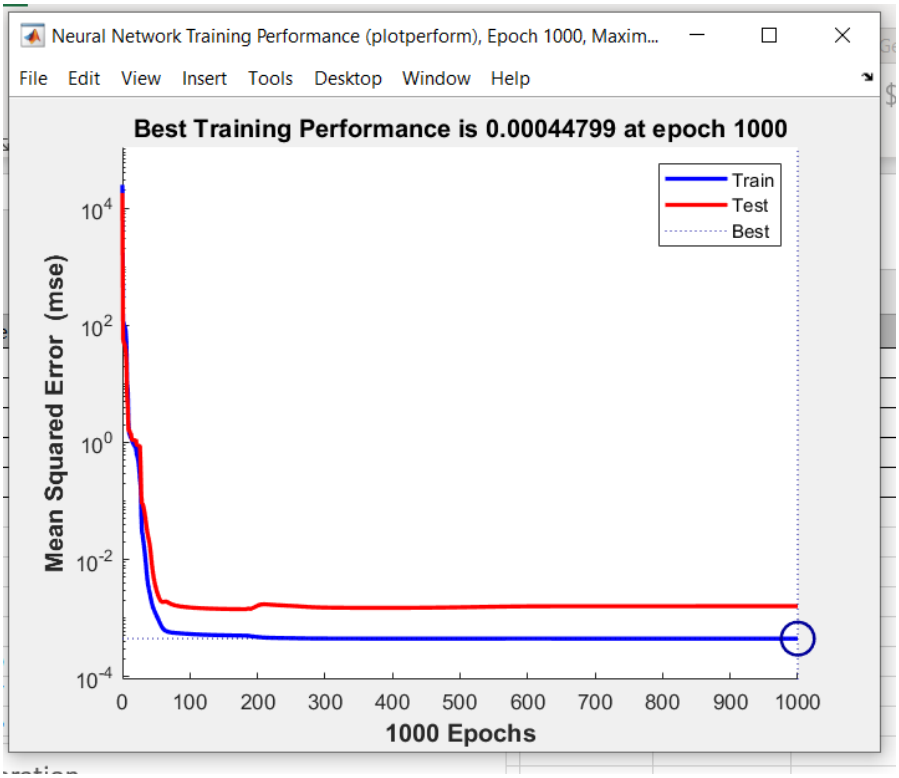

Figure 54. Mean Square Error vs Epochs graph

Upon training of the neural network, the function created now can predict cooling tower performance. The function can be found in the appendix.

15.2 Testing of Neural Network (MATLAB)

A few tests input was selected to test the neural network for accuracy and precision. Table 42 shows operating conditions for sample input. Table 43 shows the MATLAB simulation output program. Table 44 shows the neural network outlet conditions.

Table 42. Operating conditions for sample input

No. data	T_{wi} °C	T_{ai} °C	Relative Humidity %	V_{ai} m/s	m_{wi} kg/s
1	35	30	70	1.5	0.0136
2	40	30	70	2.3	0.0136
3	37	30	75	2.5	0.0142
4	35	31	76	2.75	0.0136
5	38	30	69	2.6	0.015

Table 43. MATLAB simulation program output

T_{wo} °C	T_{ao} °C	Sensible Heat W/m^2	Latent Heat W/m^2	Evaporation kg/s	Humidity kg/kg
30.47	30.22	6.59	84.16	0.01	0.02
31.65	30.38	17.10	150.30	0.01	0.02
30.92	30.25	12.14	114.99	0.01	0.02
30.44	31.09	4.96	86.57	0.01	0.02
31.00	30.28	14.08	140.69	0.01	0.02

Table 44. Neural network function output

T_{wo} °C	T_{ao} °C	Sensible Heat W/m^2	Latent Heat W/m^2	Evaporation kg/s	Humidity kg/kg
30.4	30.2	6.6	84.2	0.0122	0.0205
31.5	30.3	17.9	155.8	0.0124	0.0204
31.2	30.3	13.4	118.2	0.0125	0.0205
30.4	31.1	4.9	86.8	0.0122	0.0205
30.8	30.2	13.9	140.1	0.0124	0.0203

Figures 55 – 60 shows the MATLAB simulation against the neural network for the temperature of the water, air, sensible heat, latent heat, evaporation, and humidity.

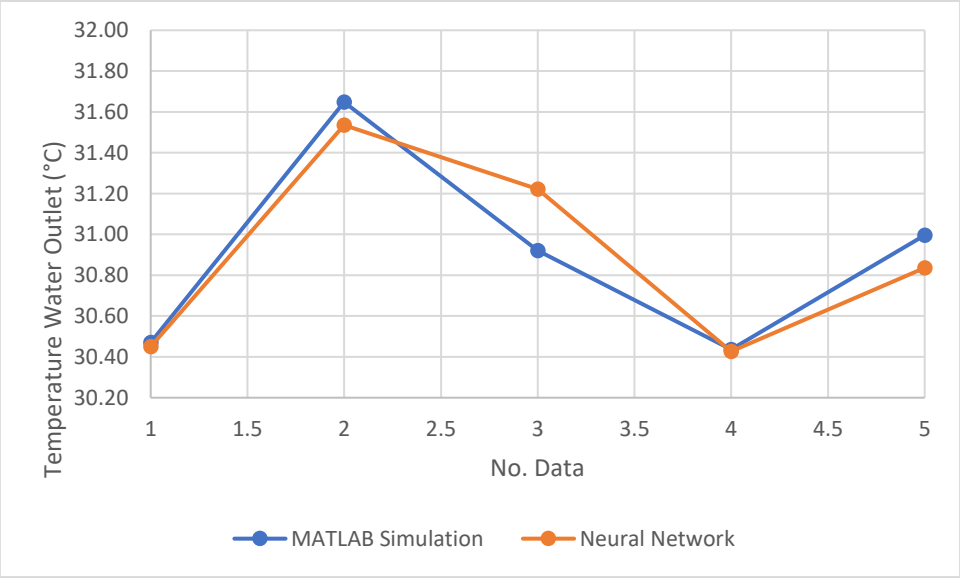

Figure 55. Water temperature output

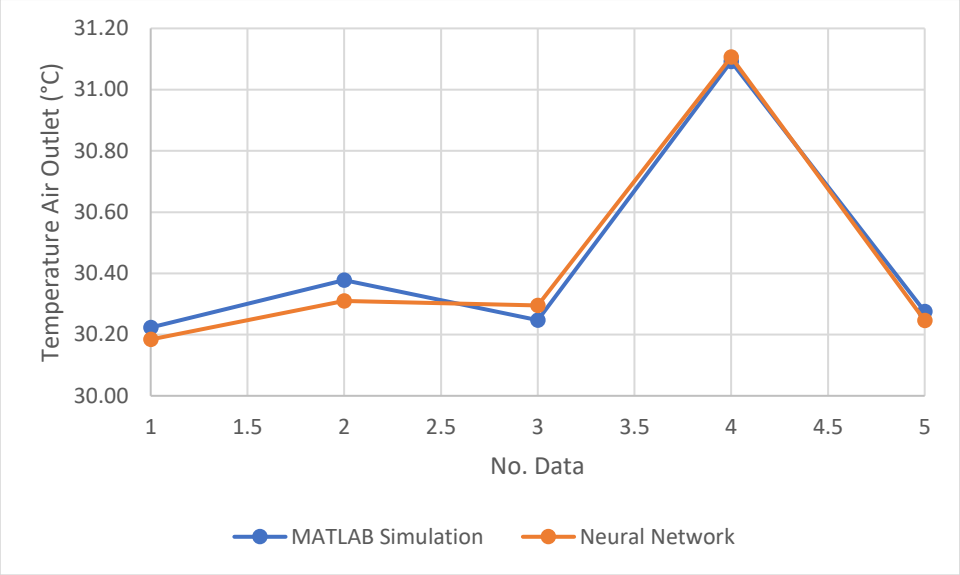

Figure 56. Air temperature output

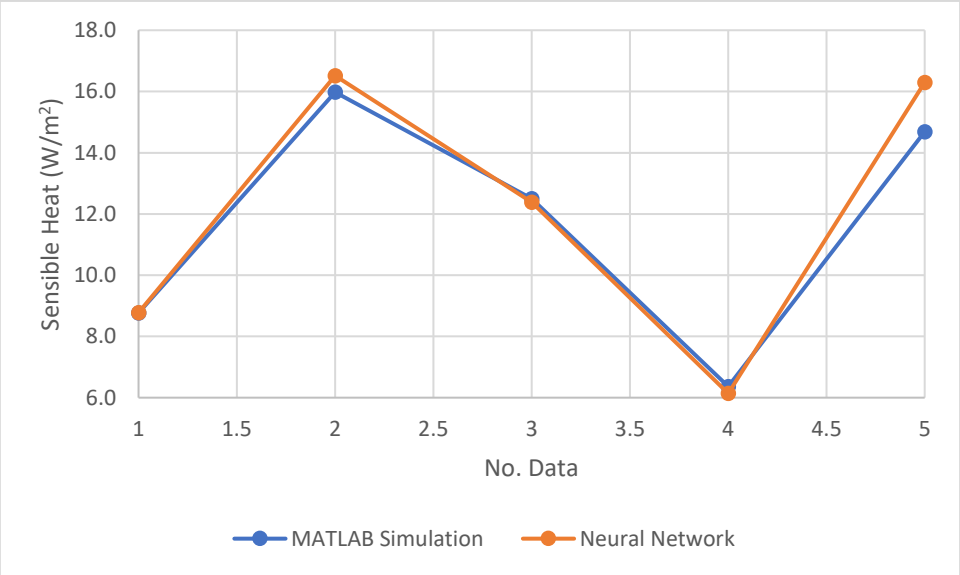

Figure 57. Sensible heat

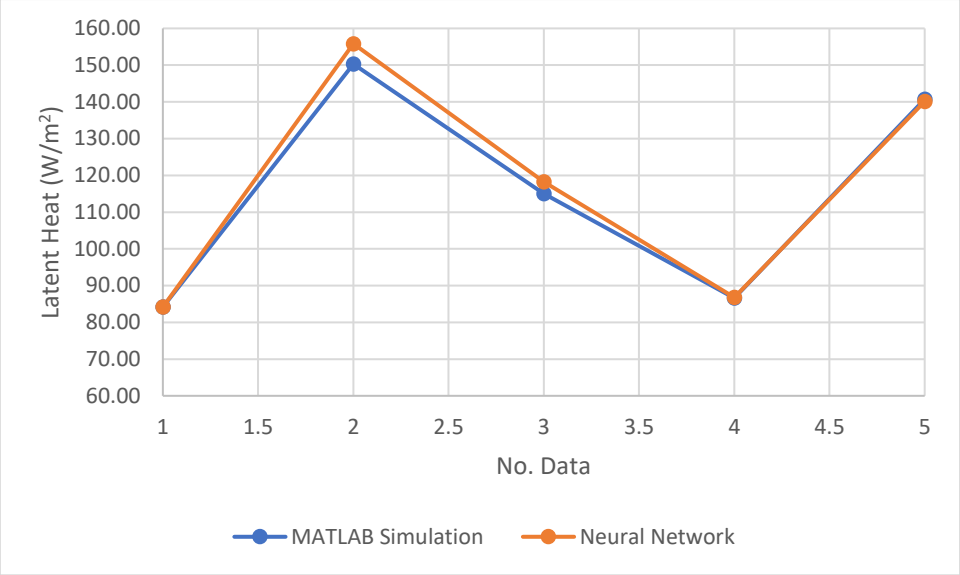

Figure 58. Latent heat

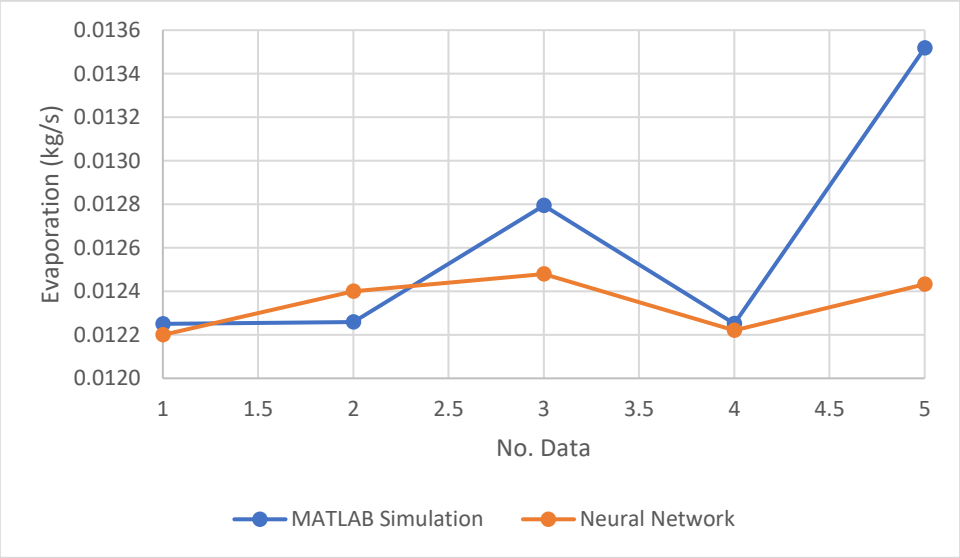

Figure 59. Evaporation

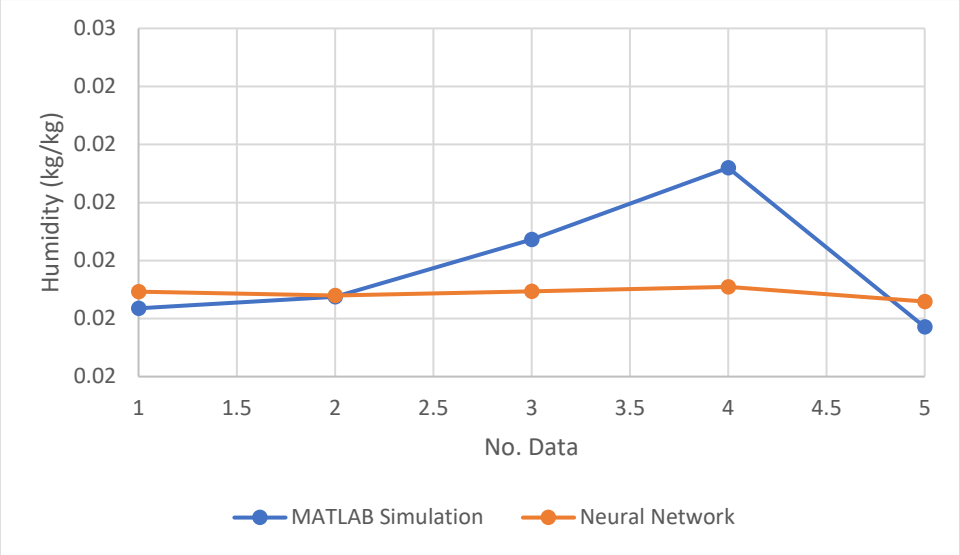

Figure 60. Humidity

The output data from neural network is compared against MATLAB simulation and percentage error was computed. From table 45, the average error for the evaporation column is within acceptable range of error of 5 – 6%. The accuracy and precision of neural networks can be further strengthened by increasing the number of datasets in input and targets or increasing the number of neurons in the network. Table 45 shows the percentage of error by comparing the simulation program with a neural network.

Table 45. Percentage of error

No. of data	T_{wo} °C	T_{ao} °C	Sensible Heat W/m^2	Latent Heat W/m^2	Evaporation kg/s	Humidity kg/kg
1	0.07%	0.13%	0.19%	0.00%	0.41%	1.42%
2	0.36%	0.22%	4.51%	3.68%	1.15%	0.13%
3	0.97%	0.16%	10.46%	2.79%	2.46%	4.17%
4	0.03%	0.05%	1.62%	0.27%	0.24%	9.08%
5	0.51%	0.09%	1.34%	0.43%	8.02%	2.21%
Average % error	0.39%	0.13%	3.63%	1.43%	2.46%	3.40%

15.3 Neural Network (ANSYS)

A neural network setup was establish using data output from ANSYS. Since ANSYS was unable to provide key data such as sensible heat, latent heat, and evaporation; water, air temperature, and humidity data were collected on ANSYS fluent. A total of 77 datasets were collected for the neural network dataset.

15.4 Neural Network setup and testing (ANSYS)

Neural network setup was like the setup of a neural network using MATLAB program data set. 50 hidden neurons were selected as it provides the best results for the training of the neural networks.

Figure 61 shows the schematic for neural network layout. Figure 62 shows the graph for mean square error; Figure 63 shows the neural network training regression graph.

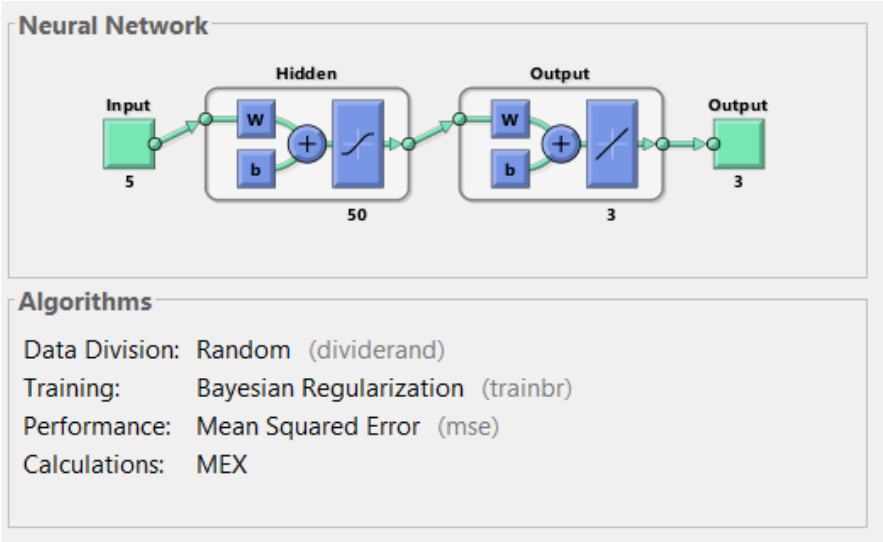

Figure 61. ANSYS neural network

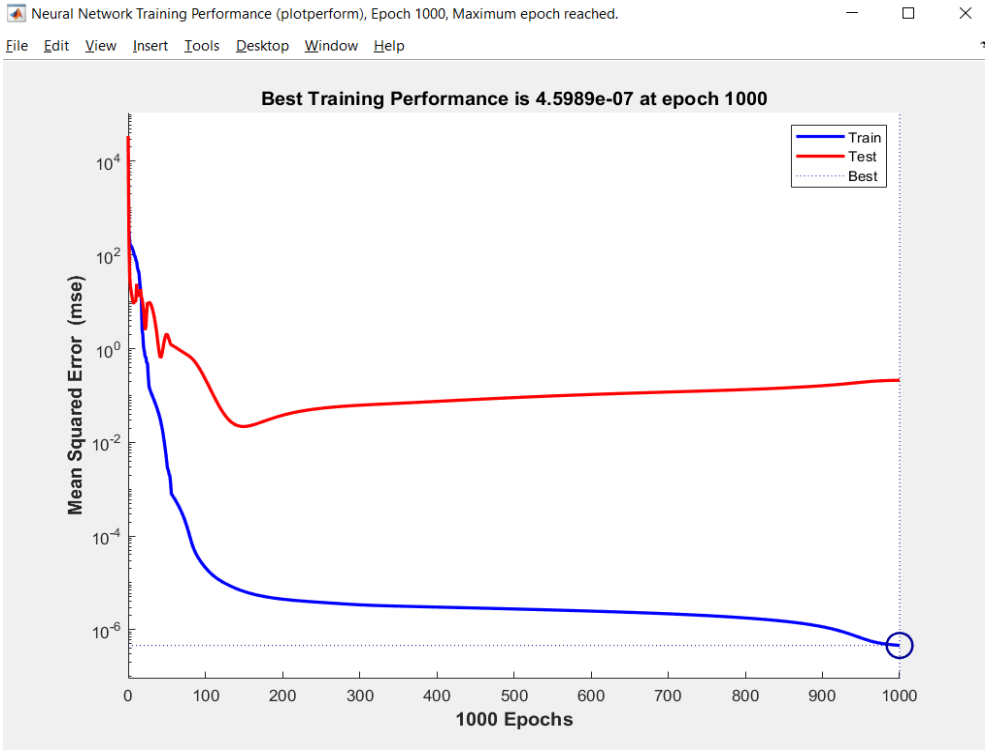

Figure 62. Mean square error vs Epoch graph

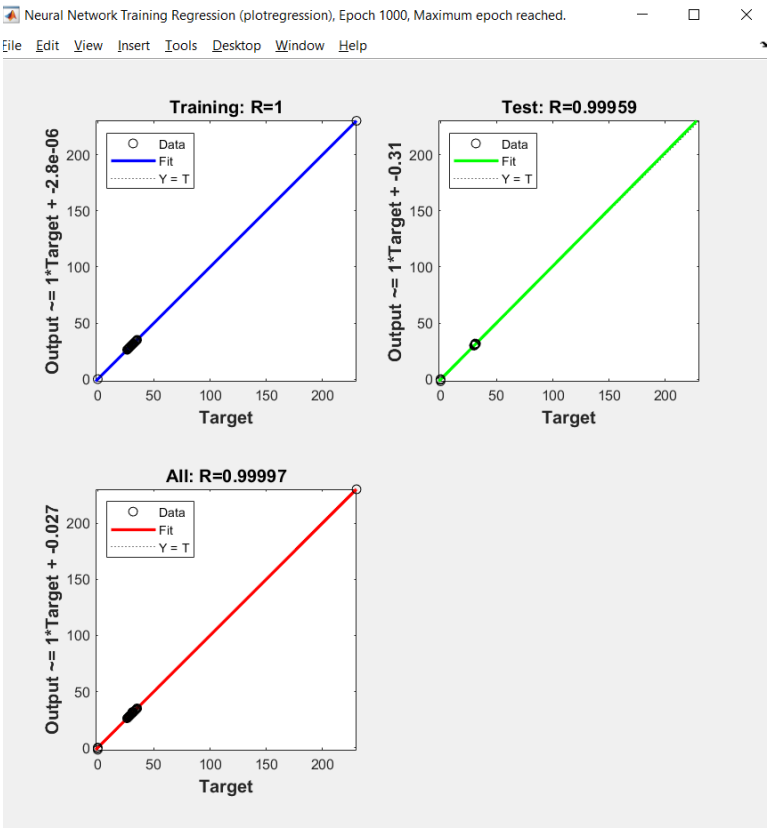

Figure 63. Neural network training regression graph

Air, water outlet temperature, and humidity are compared against the outlet conditions as presented in table 43. As seen in the table 46, the average percentage of error for ANSYS simulations is high even though the training of the neural network was successful. This could be due to insufficient meshing that results in less accurate output readings or not having enough input and target data collected for the neural networks. Hence, the neural network function created from the ANSYS dataset will not be used for the prediction of cooling tower performance.

Table 46. Percentage of error

No. data	T_{wo} °C	T_{ao} °C	**Humidity** kg/kg
1	3.33%	2.44%	0.01%
2	52.64%	4.56%	2.79%
3	1.92%	4.42%	1.29%
4	59.51%	2.74%	4.86%
5	28.33%	10.07%	19.90%
Average % error	29.15%	4.85%	5.77%

16. Comparison of MATLAB and ANSYS data

When comparing data between MATLAB and ANSYS simulation, MATLAB is accurate due to the 4th order RK method implemented and having certain assumptions to simplify the model. Thus, the MATLAB model's result would be more consistent. On the other hand, ANSYS simulation does more detailed analysis without simplified assumption. Therefore, the output would be more scattered which results in error.

17. Proposed Control Strategy

This section will propose a solution to combine the control strategies presented in the previous sections. The ambient air precooler, allows the operator to reduce ambient air temperature by 2°C. Hence, when the temperature of ambient air is high, the precooler can be activated to reduce ambient air temperature before ambient air enters the cooling tower.

In conjunction with the neural network, this allows the operator to optimize the cooling tower by changing the air inlet velocity, the mass flow rate of water, or switching on the pre-cooler to ensure that the water cooled from the cooling tower is kept at the desired temperature. Figure 64 shows a proposed control strategy schematic to optimize the cooling tower.

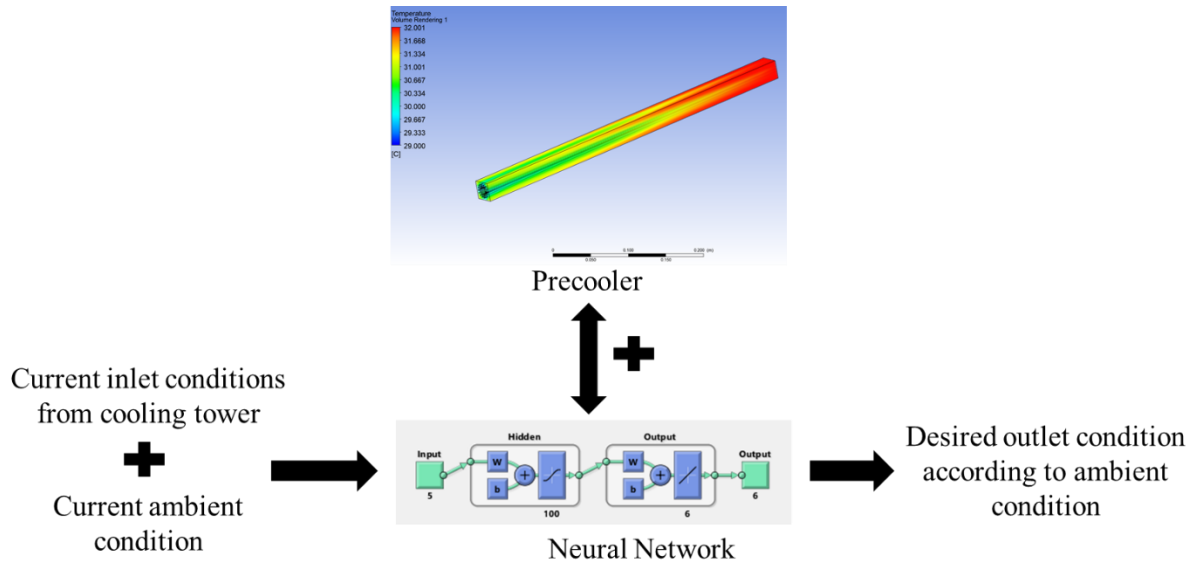

Figure 64. Control strategy schematic

With the optimization of the cooling tower to becoming more dynamic, evaporation loss and power consumption in the cooling tower would be reduced. Thus, saving water and energy consumption in the cooling towers.

18. Scenario

Under normal operating conditions, water is easily being cooled to the desired outlet temperature. However, when the ambient air temperature is high, high inlet air velocity is required to ensure that the cooling tower is continually cooling the water to the desired outlet temperature.

During a hot day, the maintenance engineer must figure out what is the optimal air velocity and water mass flow rate for the cooling tower, to ensure that water outlet is at the target temperature. To figure out the optimal air velocity and water mass flow rate for the cooling tower, the maintenance engineer must key in the new parameters and the system. From there, the engineer then computes the average value of the water temperature at the outlet from the 10*100 grids. If the outlet temperature of the water is not the desired temperature, the engineer must repeat the steps until he has found the optimal air velocity and water flow rate.

On the other hand, the neural network reduces computational effort and presents the result easily. The engineer simply keys in the desired parameters and the desired output values will be computed. This step takes less than 20 seconds to be completed. In addition, if the ambient air temperatures are high, the pre-cooler can be activated to reduce the air temperature by 2°C. For air inlet temperature at 32°C at 70% relative humidity with fixed inlet parameters, to cool water to the desired temperature of 29°C, inlet air velocity would be 8m/s. This inlet velocity is over the typical inlet ranged suggested by published literature. On the other hand, with the activation of an ambient air pre-cooler, the is air velocity is reduced from 8m/s to 3.5m/s. Table 46 shows the inlet operating conditions to cool water from 35°C to 29°C.

Table 46. Comparison between pre-cooler and without pre-cooler

			Pre-cooler	Without Pre-cooler
Inlet parameters	T_{wi}	°C	35.0	35.0
	T_{ai}	°C	30.0	32.0
	mf	kg/kg	0.0180	0.0180
	RH	%	70.0	70.0
	V_{ai}	m/s	3.5	8.0
	ma_{wi}	kg/s	0.0136	0.0136
Outlet parameters	T_{wo}	°C	29.0	29.0

19. Conclusion

In conclusion, the most optimal design for ambient air precoolers is the counterflow configuration with 16 fins. The chosen configuration can cool ambient air from up to 2 °C. The neural network developed on MATLAB reduces computational time which saves time and effort. The ambient air-precooler can reduce air inlet power consumption by half during hot days.

The ambient air precooler and neural network developed on MATLAB can be used in conjunction to save time and reduce energy consumption. The proposed solution provides the operator insights on when to increase or reduce inlet velocity, flow rates or even switching on ambient air cooler when the ambient air temperature is high.

20. Future Works/Studies

Other configurations of the cooling tower fill pack could not be investigated in-depth as each set of configurations designed on ANSYS would require a new set of setup parameters. Hence, more time will be required to fully configure the simulation set up correctly. By creating different types of configurations on ANSYS, the heat transfer coefficient can be found on ANSYS. The heat transfer coefficient can then be used and in the MATLAB program. Next, the neural network function can then be re-modelled this makes the neural network more accurate and precise for real-world application. Lastly, data from other tropical climates such as Malaysia, Thailand, Indonesia, etc. can be used to train the neural network function to further enhance the network to be more robust and dynamic in predicting cooling tower performance.

In addition, an appdesigner function on MATLAB can be explored to create a user-friendly interface. Examples of other configurations can be seen in the appendix.

21. Nomenclature

C_p	specific heat at constant pressure (kJ/kg-K)	Subscripts	
$\dot{m}$	mass flux (kg/m^{2}s)	a	Air
T	Temperature (°C)	w	Water
A	Area (m)	d	Change in a small area
h_m	Mass transfer coefficient (kg/m^{2}s)	v	Water Vapor
h_c	Convective heat transfer coefficient (W/m^2.K)	i	Inlet
h_{fg}	Latent heat of vaporization (kJ/kg)	o	Outlet
mf_{is}	Mass fraction of water vapor at the saturated section of water film	s/sat	Saturated
m_{fia}	Mass fraction of water vapor in the air (kg/kg)	wb	wet bulb
Qs	Sensible heat transfer (W/m^2)		
Q_L	Latent heat transfer (W/m2)		
ρ	Density (kg/m^3)		
M	mass (kg)		
RH	Relative Humidity (%)		
x	dryness fraction		
ω	humidity (%)		
Δ	Small change in		

22. APPENDIX

22.1 Data range used for MATLAB Neural Network

Detailed Range of Database						Typical Condition							Units
T_{wi}	30	31	32	33	34	35	36	37	38	39	40	40	°C
T_{ai}	25	26	27	28	29	30	31	32	33	34	35	35	°C
mf	0.0145	0.0152	0.0159	0.0166	0.0173	0.018	0.019	0.020	0.022	0.024	0.026	0.026	kg/kg
ω	50	54.5	59.0	63.5	68.0	70	72.5	77.0	81.5	86.0	90.5	95	%
V_{ai}	1	1.35	1.7	2.05	2.4	2.75	3.1	3.45	3.8	4.15	4.5	4.5	m/s
$\dot{m}_{wi}$	0.0062	0.0077	0.0092	0.0106	0.0121	0.0136	0.0151	0.0166	0.0180	0.0195	0.0210	0.0210	kg/s
	0.0021	0.0026	0.0031	0.0035	0.0040	0.0045	0.0050	0.0055	0.0060	0.0065	0.0070	0.0070	kg/m^2.s
	0.0062	0.0077	0.0092	0.0106	0.0121	0.0136	0.0151	0.0166	0.0180	0.0195	0.0210	0.0210	kg/m of width.s

22.2 Various fill Configurations designed in ANSYS

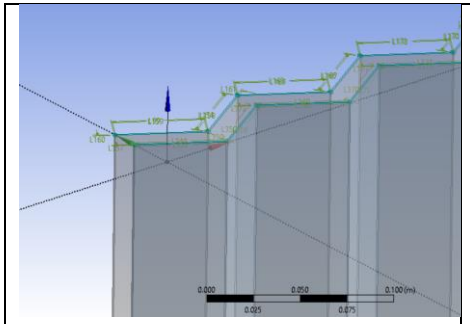	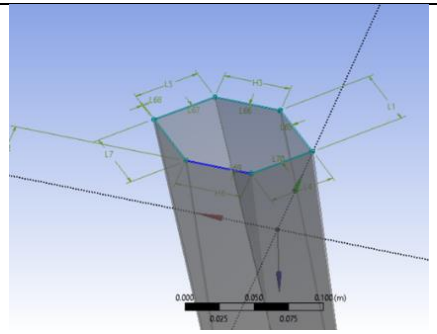	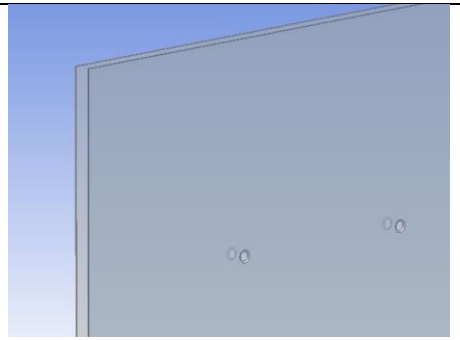	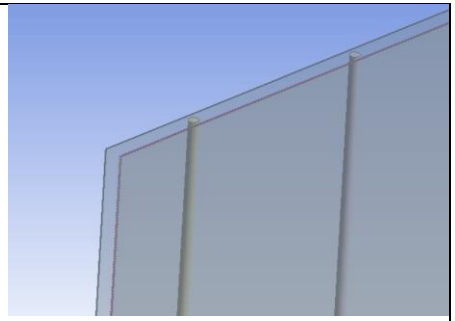
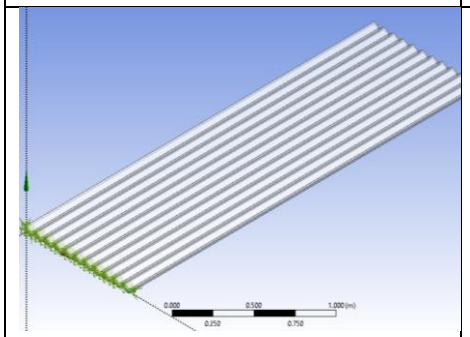	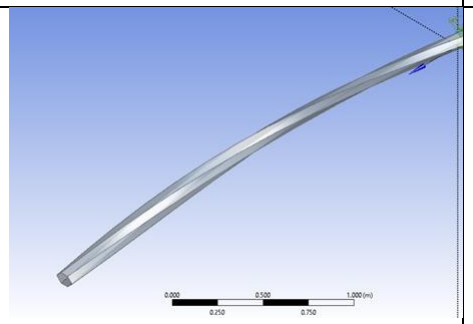	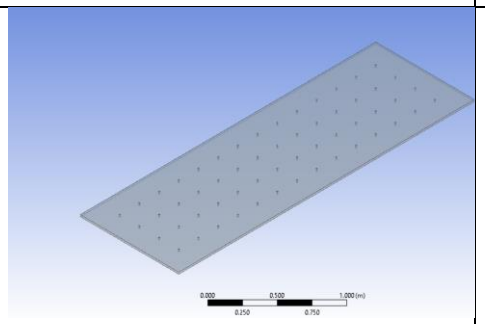	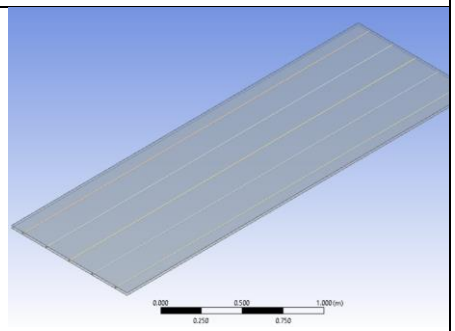
Corrugated crossflow fill	Honeycomb counterflow fill	Dimpled plate crossflow fill	Indirect contact crossflow fill

23. REFERENCES

1. P. Shahali, M. Rahmati, S. R. Alavi, and A. Sedaghat, “Experimental study on improving operating conditions of wet cooling towers using various rib numbers of packing,” *International Journal of Refrigeration*, vol. 65, pp. 80–91, Jan. 2016.
2. A. Mirabdolah Lavasani, Z. Namdar Baboli, M. Zamanizadeh, and M. Zareh, “Experimental study on the thermal performance of mechanical cooling tower with rotational splash type packing,” *Energy Conversion and Management*, vol. 87, pp. 530–538, Aug. 2014.
3. R. Javadpour, S. Zeinali Heris, and Y. Mohammadfam, “Optimizing the effect of concentration and flow rate of water/ mwcnts nanofluid on the performance of a forced draft cross-flow cooling tower,” *Energy*, vol. 217, p. 119420, Nov. 2020.
4. R. Javadpour, S. Zeinali Heris, and Y. Mohammadfam, “Optimizing the effect of concentration and flow rate of water/ mwcnts nanofluid on the performance of a forced draft cross-flow cooling tower,” *Energy*, vol. 217, p. 119420, Nov. 2020.
5. J. Yang, K. T. Chan, X. Wu, X. Yang, and H. Zhang, “Performance enhancement of air-cooled chillers with water mist: Experimental and analytical investigation,” *Applied Thermal Engineering*, vol. 40, pp. 114–120, Feb. 2012.
6. R. Ghosh, C. Patra, P. Singh, R. Ganguly, R. P. Sahu, I. Zhitomirsky, and I. K. Puri, “Influence of metal mesh wettability on fog harvesting in industrial cooling towers,” *Applied Thermal Engineering*, vol. 181, p. 115963, Aug. 2020.
7. A. Alkhedhair, I. Jahn, H. Gurgenci, Z. Guan, and S. He, “Parametric study on spray cooling system for Optimising nozzle design WITH pre-cooling application in natural draft Dry cooling towers,” *International Journal of Thermal Sciences*, vol. 104, pp. 448–460, Apr. 2016.
8. R. Zhao, S. Bu, X. Zhao, L. Zhang, W. Xu, Z. Yu, J. Fang, Y. Ji, Y. Hu, and B. Bao, “Study on thermal performance of new finned heat exchange tube bundles in cooling tower,” *International Journal of Thermal Sciences*, vol. 168, p. 107064, May 2021.
9. Z. Yu, C. Sun, L. Zhang, B. Bao, Y. Li, S. Bu, and W. Xu, “Analysis of a novel combined heat exchange strategy applied for cooling towers,” *International Journal of Heat and Mass Transfer*, vol. 169, p. 120910, Jan. 2021.
10. A. V. Dmitriev, I. N. Madyshev, V. V. Kharkov, O. S. Dmitrieva, and V. E. Zinurov, “Experimental investigation of fill pack impact on thermal-hydraulic performance of evaporative cooling tower,” *Thermal Science and Engineering Progress*, vol. 22, p. 100835, Dec. 2020.
11. M. Shublaq and A. K. Sleiti, “Experimental analysis of water evaporation losses in cooling towers using filters,” *Applied Thermal Engineering*, vol. 175, p. 115418, May 2020.
12. N. Gilani, A. Doustani Hendijani, and R. Shirmohammadi, “Developing of a novel water-efficient configuration for shower cooling tower integrated with the liquid desiccant cooling system,” *Applied Thermal Engineering*, vol. 154, pp. 180–195, Mar. 2019.

13. M. Amini, M. Zareh, and S. Maleki, “Thermal performance analysis of mechanical draft cooling tower filled with rotational splash type packing by using nanofluids,” *Applied Thermal Engineering*, vol. 175, p. 115268, Aug. 2014.
14. A. C. B. Thomé, P. G. Santos, and A. G. Fisch, “Using rainwater in cooling towers: Design and performance analysis for a petrochemical company,” *Journal of Cleaner Production*, vol. 224, pp. 275–283, Mar. 2019.
15. S. Taghian Dehaghani and H. Ahmadikia, “Retrofit of a wet cooling tower in order to reduce water and fan power consumption using a wet/dry approach,” *Applied Thermal Engineering*, vol. 125, pp. 1002–1014, Jul. 2017.
16. X. Fan, X. Lu, H. Nie, H. Zhu, Q. Wang, Y. Kang, S. Liu, X. Zheng, Z. Liu, Y. Zhang, X. Long, and J. Li, “An experimental study of a novel dew point evaporative cooling tower based on m-cycle,” *Applied Thermal Engineering*, vol. 190, p. 116839, Mar. 2021.
17. A. C. C. Tomás, S. D. O. Araujo, M. D. Paes, A. R. M. Primo, J. A. P. Da Costa, and A. A. V. Ochoa, “Experimental analysis of the performance of new alternative materials for cooling tower fill,” *Applied Thermal Engineering*, vol. 144, pp. 444–456, Aug. 2018.
18. R. Kumar, P. L. Dhar, and S. Jain, “Development of new wire mesh packings for improving the performance of Zero carryover spray tower,” *Energy*, vol. 36, no. 2, pp. 1362–1374, Dec. 2010.
19. A. K. Tiwari, S. Jain, and S. Karmakar, “An improved three-dimensional numerical model of a V-bar splash fill in a wet cooling tower,” *International Communications in Heat and Mass Transfer*, vol. 128, p. 105617, Sep. 2021.
20. E. Hajidavalloo, R. Shakeri, and M. A. Mehrabian, “Thermal performance of cross flow cooling towers in variable wet bulb temperature,” *Energy Conversion and Management*, vol. 51, no. 6, pp. 1298–1303, Feb. 2010.
21. P. J. Grobbelaar, H. C. R. Reuter, and T. P. Bertrand, “Performance characteristics of a trickle fill in cross- and counter-flow configuration in a wet-cooling tower,” *Applied Thermal Engineering*, vol. 50, no. 1, pp. 475–484, Jun. 2013.
22. P. Abraham, M. H. Sharqawy, and M. E. Shawkat, “Thermal and hydraulic characteristics of multiple row spiral finned tube heat exchangers,” *International Journal of Refrigeration*, vol. 130, pp. 56–66, May 2021.